ABSTRACT

Title of thesis: A VLSI Design for Phase Synchronization of Two Globally Coupled Oscillators

Hua Luo, Master of Science, 2017

Thesis directed by: Professor Robert W. Newcomb
Department of Electrical and Computer Engineering

Phase synchronization of globally coupled oscillators is a common phenomenon in almost every branch of science including chemistry, physics, astronomy, biology, and electronics. It has various applications such as laser arrays, chemical and electrical oscillators, metronomes, pathological synchronization in Parkinson's disease, and synchronized oscillation of neurons. In this thesis, we study and design globally coupled oscillators with a focus on biological applications.

We mathematically analyze one of the most widely studied models of globally coupled oscillators proposed by Matthews et al.. Based on this model, we design two globally coupled oscillator systems in Simulink. Simulation results show that our systems work perfectly as synchronized globally coupled oscillators.

We then design a two-channel globally coupled oscillator system with integrated circuits using ON Semiconductor's 0.5 μm CMOS technology and a ± 5 V power supply. Simulation results in PSpice show that the two channels get synchronized in less than one cycle and they can oscillate at frequencies less than 1 Hz.

A VLSI Design for Phase Synchronization of Two Globally Coupled Oscillators

by

Hua Luo

Thesis submitted to the Faculty of the Graduate School of the
University of Maryland, College Park in partial fulfillment
of the requirements for the degree of
Master of Science
2017

Advisory Committee:
Professor Robert W. Newcomb, Chair/Advisor
Professor A. Yavuz Oruc
Professor Mark Austin

Acknowledgments

I owe my gratitude to all the people who have helped me in my study and life. I will cherish these memories forever.

First of all, I would like to thank my advisor, Professor Robert W. Newcomb. He is a great professor who cares about his students. Whenever I encounter difficulties, he always gives me many insightful suggestions. It has been really a pleasure and an honor to work with him. He is also a kind friend. He always helps me and many other students with other problems in life, no matter how trivial they seem. Above all, he is an extraordinary person. I feel so honored and lucky to get to know him and work with him.

I would also like to thank Professor A. Yavuz Oruc and Professor Mark Austin for serving on my thesis committee. Both of them have really busy schedules. But they spared their precious time to review my manuscript.

I would like to thank staff members Bill Churma, Melanie Prange, Emily Erwin, Maria Hoo, and Vivian Lu for helping me with many things like registration, payroll, graduation, teaching assistant assignment, and so on. They make the life of many graduate students in the Electrical and Computer Engineering department much easier, and happier.

I want to thank everyone who helped me becoming a good teaching assistant. The first time being a teaching assistant is hard. But they made this process much easier for me. Shyam Mehrotra and Bryan Quinn are always there to help anyone. Yumeng Cui is such an experienced and helpful teaching assistant. I would also

like to thank all my students. I could not have completed all my jobs without their support.

The Clark School of Engineering and the department of Electrical and Computer Engineering offered me scholarships and teaching assistant positions. Without these financial support, it would not have been possible for me to come to the United States and finish my study here.

I would like to thank my friends, Xiaoxu Meng, Shang Li, and so on. Adapting to the new life here is challenging, they offered help in many ways and shared their experience with me. They make me feel connected, not alone.

I owe my deepest thanks to my family. For the past 26 years, they have always loved me and supported me. Even though I was born in a remote and poor village, they have always encouraged me to pursue my dreams.

It is impossible to recall the names of all the people who have helped me at this moment. But I do appreciate everything everyone has done.

Table of Contents

List of Figures vi

List of Abbreviations vii

1 Introduction 1
- 1.1 Globally Coupled Oscillators . . . 1
- 1.2 Related Works . . . 2
- 1.3 Contributions . . . 4
- 1.4 Organization . . . 5

2 Mathematical Models for Globally Coupled Oscillators 6
- 2.1 Different Models . . . 6
- 2.2 Two-channel Globally Coupled Oscillators . . . 8
- 2.3 Chapter Summary . . . 11

3 Model Verification Using Simulink 13
- 3.1 Implementation with Amplitude and Phase . . . 13
  - 3.1.1 System Modeling . . . 13
  - 3.1.2 Simulation Results . . . 15
- 3.2 Implementation with Real and Imaginary Parts . . . 18
  - 3.2.1 System Modeling . . . 18
  - 3.2.2 Simulation Results . . . 19
- 3.3 Chapter Summary . . . 20

4 Oscillator System Design and Implementation with CMOS Circuits 23
- 4.1 Overall Specifications . . . 23
- 4.2 Subcircuit Design . . . 24
  - 4.2.1 Integrators . . . 24
  - 4.2.2 Wide Input Range Multipliers . . . 27
  - 4.2.3 Current Mirrors . . . 36
  - 4.2.4 Operational Transconductance Amplifiers . . . 42
- 4.3 A Two-Channel Globally Coupled Oscillator System . . . 53
  - 4.3.1 Circuit Implementation . . . 53

4.3.2 Simulation Results 54
4.4 Chapter Summary 56

5 Conclusions and Future Work 58
5.1 Main Contributions 58
5.2 Future Work 59

A Transistor Sizes 60

Bibliography 61

List of Figures

3.1 An oscillator system in Simulink. 14
3.2 Time domain response of r_1 and r_2. 15
3.3 Time domain response of φ_1 and φ_2. 16
3.4 Time domain response of x and y. 17
3.5 How r changes as ω_2 changes with $\omega_1 = 1$ and $K = 2$. 18
3.6 Time domain response of φ_1 and φ_2 for $\omega_2 = 0.5$ and 1.5, $K = 2$. . . 19
3.7 New oscillator system in Simulink. 21
3.8 New time domain response of x and y. 22

4.1 Typical continuous time integrator. 25
4.2 Basic idea of multipliers. 29
4.3 Four quadrant multiplier basic architectures. (a) Using single quadrant multipliers. (b) Using square devices. 29
4.4 A MOS Gilbert multiplier. 32
4.5 Attenuators. (a) Proposed by van Horn et al.. (b) Modified for our oscillator. 35
4.6 The multiplier for our oscillator. 36
4.7 Current mirros. (a) Basic current mirror. (b) Cascode current mirror. 37
4.8 Current mirrors used in our circuit. 39
4.9 Output waveform of one multiplier connected to one current mirror. . 41
4.10 Transfer characteristics of our multiplier. 42
4.11 Transfer characteristics for inputs in [-1,1]. 43
4.12 Schematic symbol for: (a) an op-amp (b) an OTA. 44
4.13 Open-loop and closed-loop applications of operational amplifiers. (a) Comparator. (b) Non-inverting amplifier. 44
4.14 Schematic of a transconductance amplifier. 47
4.15 Schematic of transconductance amplifiers. 51
4.16 Transfer characteristic curve of our transconductance amplifier. . . . 52
4.17 One channel of the oscillator. 54
4.18 Time domain response of our oscillator. 55
4.19 Time domain response comparison. 57

List of Abbreviations

CMOS	Complementary Metal-Oxide-Semiconductor (CMOS)
MOSFET	Metal-Oxide-Semiconductor Field-Effect Transistor
OTA	Operational Transconductance Amplifier
AC	Alternating Current
VLSI	Very Large Scaled Integrated Circuits

Chapter 1: Introduction

1.1 Globally Coupled Oscillators

In 1665 Christiaan Huygens, the inventor of the pendulumn clock, found that two pendulumn clocks hanging side by side in his room always swang in perfect synchrony [1,2]. Even if he tried to break this balance, they would regain synchrony after some time. He concluded that there must be some interaction between the two clocks. He also found that if they were placed at opposite sides of the wall, they would not become synchronized. Huygens's observation led to a new area of research: the study of coupled oscillators [2]. Also in the 17th century, German naturalist, physician, and explorer Engelbert Kaempfer noticed the synchronization among fireflies during his visit to Southeast Asia [3]. Later in his book [4], he described that after a group of fireflies settled on a tree, they "sometimes hide their light all at once, and a moment after make it appear again with the utmost regularity and exactness". Since then, there has been a lot of research in the synchronization of fireflies [5–11]. One can even use artificial lights to interfere with fireflies and affect the frequency they flash [12]. As time goes by, people find more and more coupled oscillation phenomena in the natural world, like the formation flight of migrating birds [13], menstrual synchrony and suppression [14], animal locomotion [15], and

pedestrian' synchrony on the bridge [16–19].

In the past few centuries, coupled oscillators have been widely studied in almost every branch of science including chemistry, physics, astronomy, quantum electronics, and biology. They are found in various applications such as laser arrays [20–24], Josephson junctions [25–27], chemical and electrochemical oscillators [28–32], metronomes [33, 34], and pathological synchronization in Parkinson's disease [35]. Therefore, controlling these coupled oscillators and breaking/achieving synchronization can be very useful for engineering systems design and medical treatment for certain conditions [36].

1.2 Related Works

To understand the behavior of coupled oscillators, scientists have been seeking tractable mathematical models for decades. Among them, Arthur Winfree proposed one of the earliest mathematical models for collective synchronization [37, 38] in 1967. Assuming that the interaction between different oscillators in the system is 'weak' and thus does not affect the oscillating amplitude, only phase variation needs to be considered [3]. When the coupling between oscillators goes beyond a certain threshold, some of them become synchronized at a common frequency. This is a milestone in the study of coupled oscillators. However, the model Winfree proposed is hard to solve mathematically in its full generalized form [39], although Ariaratnam and Strogatz proposed a solvable version of Winfree's model years later [40]. Therefore, researchers have been seeking other models.

A few years later, Yoshiki Kuramoto reformulated this model and presented the famous Kuramoto model [28, 41]. The Kuramoto model discusses systems of N coupled phase oscillators and simplifies the coupling between different oscillators with a sine function of their phase differences. Unlike Winfree's model, the Kuramoto model is solvable. At the same time, it is also complex enough to represent various phenomena. Therefore, the Kuramoto model has been widely studied since then [39, 42–58]. In 1991, Matthews et al. generalized the Kuramoto model by taking into consideration of amplitude change [59]. This is a remarkable breakthrough. In reality, many coupled oscillator systems do show variations in amplitude. Their model brought up many new findings, the most important one being that the system can enter an unsteady state.

It is worth noting that all the above works are done by theoretical scientists, and few people have made any hardware based on the Kuramoto model, or Matthews's model. In this thesis we focus on biological applications such as pathological synchronization in Parkinson's disease, and synchronized oscillation of neurons. In the circuit design area, people have designed a lot of coupled oscillators [60–65]. But they are inductor-capacitor(LC) oscillators focused on electrical applications such as wireless networking, radio-frequency transceivers, digital communication systems, and so on. For most of them, the coupling between different oscillators is simplified for that specific application. Therefore we cannot use these coupled LC oscillators directly for studying other phenomena with more complex coupling between different oscillators. Another important reason we want to seek alternatives is that, since they are LC oscillators, their working frequencies are very

high. They can vary from the order of kHz to the order of GHz. This is a great advantage for them in their applications, but not for our scenario. For the biological applications mentioned earlier, the oscillating frequencies can be very low. Scientists have reported pathological oscillations of 3 Hz to 6 Hz parkinsonian tremor [66] and neuron oscillations in the range of 10 Hz to 50 Hz [67]. Working at such low frequencies is almost impossible for LC oscillators because that would require really huge capacitors, which is infeasible.

1.3 Contributions

In this thesis we will study the mathematical model of globally coupled oscillators proposed by Matthews et al. [59]. We use Simulink to verify their model. We will also design a globally coupled oscillator system using integrated circuits based on that model. The main contributions are listed below:

- We mathematically analyze the model proposed by Matthews et al. (Chapter 2). Based on this model, we simulate two coupled oscillator systems using Simulink (Chapter 3). Simulation results show that our systems work perfectly as globally coupled oscillators.

- We design and implement a two-channel globally coupled oscillator system with integrated circuits (Chapter 4). Using ON Semiconductor's 0.5μm CMOS technology and a $\pm$5 V power supply, the system fully functions. Simulation results in PSpice show that the two channels become synchronized in less than one cycle and they can oscillate at frequencies to the order of, or even less than,

1 Hz.

1.4 Organization

. Chapter 2 will discuss mathematical models of globally coupled oscillators and then analyze the model proposed by Matthews et al. In Chapter 3, we will simulate two coupled oscillator systems using Simulink. Chapter 4 will present the design and implementation of a two-channel globally coupled oscillator system designed with integrated circuits. Chapter 5 will conclude this thesis and give suggestions for possible future works.

Chapter 2: Mathematical Models for Globally Coupled Oscillators

In this chapter, we will briefly discuss the three different models for globally coupled oscillators mentioned in Chapter 1. And we will go into more depth about the model proposed by Matthews et al. [59] when the number of oscillators in the system is two.

2.1 Different Models

The first mathematical model for globally coupled oscillators to be discussed is that of Arthur Winfree [37,38]. He reduced the dynamics of each oscillator/channel to only one variable, the phase φ. Let N denote the number of oscillators ($N \gg 1$), the model can be written as:

$$\frac{d\varphi_k}{dt} = \omega_k + \frac{\epsilon}{N}\Gamma(\varphi_k)\sum_{i=1}^{N} I(\varphi_i). \tag{2.1}$$

Here $k = 1, 2, ..., N$. ϵ stands for the coupling strength between different channels, and ω_k is the natural frequency of each channel. $\Gamma(\varphi_k)$ describes one channel's phase sensitivity to purtubation, and is usually called the phase response curve. In reality, the phase response curve can be determined by repeating experiments and collecting data from one isolated system [3]. $I(\varphi_i)$ reflects how the phase of one oscillator affects another. Note that Γ and I are global functions in that they are

the same for different channels. Therefore, the main difference between different channels is their different natural frequencies. Although this model is not known to be solvable in its general form, it is a milestone in the study of coupled oscillators.

The Kuramoto model is actually very similar to the model proposed by Winfree, as described by the equation below [28, 41]:

$$\frac{d\varphi_k}{dt} = \omega_k + \sum_{i=1}^{N} K_{ki} \sin(\varphi_i - \varphi_k), \tag{2.2}$$

where $k = 1, 2, ..., N$, and ω_k is the natural frequency of each channel. From the equation above, it is clear that the Kuramoto model uses a sine function and a matrix K_{kj} to describe the coupling between different channels as well as one channel's sensativity to pertubation. In Winfree's model, the function I can be very complex. Kuramoto simplified it with a sine function. In addition, he used a matrix K_{kj} to replace items Γ and $\frac{\epsilon}{N}$. As a result, this model is solvable and still sufficient to describe many phenomena. There are different models for the matrix K_{kj}, such as hierarchical coupling, short-range coupling, random long-range coupling, and state-dependent coupling, as discussed in [39].

In this thesis, we will focus on the model proposed by Matthews et al. [59], which is a generalized version of the Kuramoto model. As mentioned in Chapter 1, this model also describes the variation in oscillating amplitude. Each independent oscillator in the system is described by the following equation:

$$\frac{dz_k}{dt} = (1 - |z_k|^2 + j\omega_k) z_k, \tag{2.3}$$

where $k = 1, 2, ..., N$. ω_k is the natural frequency of each channel, and j is the imaginary unit ($\sqrt{-1}$). In this model, z_k stands for one oscillator's position in the

complex plane. It considers both amplitude and phase. z_k is normalized such that when there is no coupling, each channel has a stable limit cycle of 1. Then Matthews et al. took the coupling between different channels as a linear function, and got the following model for a system of N globally coupled oscillators:

$$\frac{dz_k}{dt} = (1 - |z_k|^2 + j\omega_k)z_k + \frac{K}{N}\sum_{i=1}^{N}(z_i - z_k) \tag{2.4}$$

where $k = 1, 2, ..., N$. K is a constant standing for the coupling strength between different channels. In this model, different channels affect each other by a linear function of their position difference in the complex plane. This model may look quite different from the Kuramoto model at first glance. But when we go into more depth in the next section, we will show that there are many similarities and connections between them.

2.2 Two-channel Globally Coupled Oscillators

When designing an actual circuit, or doing Simulink simulation, it is impossible to simulate a system of infinite number of coupled oscillators. Therefore, in the rest of this thesis we focus on the case of two-channel globally coupled oscillators. Although two is not a large number, it is sufficient to demonstrate many properties suggested by the previous models.

When N is 2, Equation 2.4 becomes:

$$\frac{dz_k}{dt} = (1 - |z_k|^2 + j\omega_k)z_k + \frac{K}{2}(z_i - z_k) \tag{2.5}$$

where $k = 1, 2, i = 3 - k$. A complex number z can be written as $z = re^{j\varphi}$, where r and φ stand for its amplitude and phase, respectively. Plugging this into

Equation 2.5, we have:

$$\begin{aligned} \frac{dr_k}{dt} &= (1 - r_k^2) r_k + \frac{K}{2}[r_i \cos(\varphi_i - \varphi_k) - r_k] \\ \frac{d\varphi_k}{dt} &= \omega_k + \frac{K}{2}\frac{r_i}{r_k}\sin(\varphi_i - \varphi_k) \end{aligned} \tag{2.6}$$

where $k = 1, 2, i = 3 - k$. Recall that the equation for the Kuramoto model is

$$\frac{d\varphi_k}{dt} = \omega_k + \sum_{i=1}^{N} K_{ki} \sin(\varphi_i - \varphi_k). \tag{2.7}$$

If we set N to be 2 and replace K_{ki} in Equation 2.7 with $\frac{K}{2}\frac{r_i}{r_k}$, we can get exactly the same equation as Equation 2.6. This justifies that both models are quite similar in terms of describing the phase variation. But the model proposed by Matthews et al. also incorporates amplitude changes.

Equation 2.6 gives us a more direct understanding of how the magnitude and phase of one channel is affected by those of the other one. The change in one channel's amplitude depends on itself as well as another factor linearly proportional to the phase difference between the two channels. Without coupling, how fast a channel's phase changes is determined by its own frequency only. With coupling, the two channels' magnitude and phase contribute to each other's phase change.

Moreover, using Equation 2.6, we can easily find the steady-state phase difference between the two channels. When the system becomes stable, the two channels are synchronized. Therefore, they are oscillating at the same frequency with the same magnitude. Thus their actual angular velocities are the same. So we have:

$$\begin{aligned} \frac{d\varphi_1}{dt} &= \frac{d\varphi_2}{dt} \\ r_1 &= r_2 = r \end{aligned} \tag{2.8}$$

Plugging the above equations into Equation 2.6, we get:

$$\omega_1 + \frac{K}{2}\frac{r_2}{r_1}\sin(\varphi_2 - \varphi_1) = \omega_2 + \frac{K}{2}\frac{r_1}{r_2}\sin(\varphi_1 - \varphi_2). \tag{2.9}$$

As a result:

$$\sin(\varphi_2 - \varphi_1) = \frac{\omega_2 - \omega_1}{K} \tag{2.10}$$

which gives us the value of $\varphi_2 - \varphi_1$. The steady-state phase difference between the two channels is determined by their natural frequencies and the value of coupling strength K. Similarly, We can get the steady-state oscillating amplitude r:

$$\frac{dr}{dt} = (1 - r^2)r + \frac{K}{2}[r\cos(\varphi_2 - \varphi_1) - r] = 0 \tag{2.11}$$

Solving the above equation, we get:

$$r = 0 \ or \ \sqrt{1 - \frac{K}{2}(1 - \cos(\varphi_2 - \varphi_1))} \tag{2.12}$$

which gives us the value of r. $r = 0$ represents a trivial solution where the system is not oscillating at all. Therefore we focus on the other solution. To get an explicit relationship between r, K, ω_1 and ω_2, we plug Equation 2.10 into 2.12. Then we get the following equation:

$$r = \sqrt{1 - \frac{K}{2}(1 - \cos(\arcsin(\frac{\omega_2 - \omega_1}{K})))} \tag{2.13}$$

which tells us that the steady-state oscillating amplitude depends on the value of K and the difference between ω_1 and ω_2. It should be noted that only the absolute value of $\omega_2 - \omega_1$ will affect r, which matches intuition since each channel contributes equally to the whole oscillator system.

Another aspect to look at the system via Equation 2.5 is to consider the real and imaginary parts of each channel's position in the complex plane. A complex number z can be expressed as $z = x + jy$, where x and y stand for its real part and imaginary part, respectively. Taking this into Equation 2.5, we get:

$$\begin{aligned} \frac{dx_k}{dt} &= x_k - \omega_k y_k - x_k^3 - x_k y_k^2 + \frac{K}{2}(x_i - x_k) \\ \frac{dy_k}{dt} &= y_k + \omega_k x_k - x_k^2 y_k - y_k^3 + \frac{K}{2}(y_i - y_k) \end{aligned} \tag{2.14}$$

Here $k = 1, 2, i = 3 - k$. Equation 2.14 tells us how the real and imaginary parts of one channel are affeted by themselves and those of the other channel. This is especially helpful when we design actual integrated circuits for the oscillator system described in Equation 2.5. Both Equation 2.6 and Equation 2.14 involve working with multiplicatioin and addition. However, Equation 2.6 also requires dealing with the phase difference between different channels and sine and cosine functions, which makes the circuit extremely difficult to design and implement. Therefore, it is much easier to work with voltage signals corresponding to x and y than to work with those corresponding to r and φ. When we do verification using Simulink in the next chapter, we will deal with both Equation 2.6 and Equation 2.14. But in later chapters when we design and implement the coupled oscillator system using integrated circuits, we will not trouble ourselves unnecessarily by working with Equation 2.6.

2.3 Chapter Summary

In this chapter we briefly discussed the models proposed by Winfree and Kuramoto. Then we went into more depth about the model proposed by Matthews et

al.. Specifically, we analyzed the latter model when the number of oscillators in the system is two. And we gave equations that can guide circuit design and Simulink verification.

Chapter 3: Model Verification Using Simulink

In previous chapters, we have discussed the application, background, history, as well as mathematical models for globally coupled oscillators. In this chapter, we will simulate two globally coupled oscillator systems based on the models discussed in Chapter 2 using Simulink.

3.1 Implementation with Amplitude and Phase

3.1.1 System Modeling

In chapter 2 we discussed two different ways to look at the model proposed by Matthews et al. [59]. Here we deal with r and φ first. Recall the equations for a two-channel globally coupled oscillator system are:

$$\begin{aligned} \frac{dr_k}{dt} &= (1-r_k^2)r_k + \frac{K}{2}[r_i\cos(\varphi_i-\varphi_k) - r_k] \\ \frac{d\varphi_k}{dt} &= \omega_k + \frac{K}{2}\frac{r_i}{r_k}\sin(\varphi_i-\varphi_k). \end{aligned} \tag{3.1}$$

Here $k = 1, 2, i = 3-k$. Simulink has built-in blocks for all mathematical operations we need. Thus it is quite straightforward to set up our system by replacing each operator with its corresponding block in Simulink. The whole coupled oscillator system is shown in Figure 3.1.

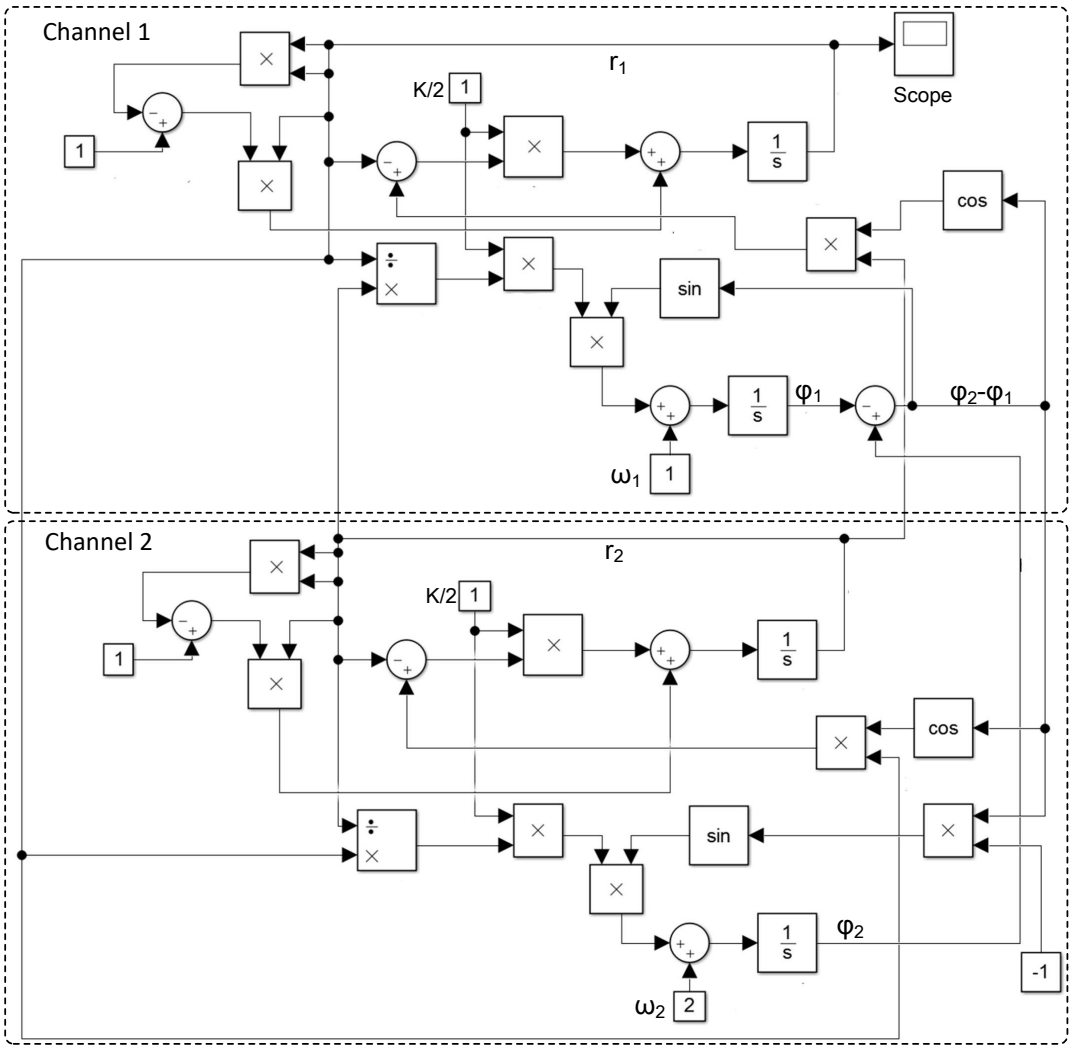

Figure 3.1: An oscillator system in Simulink.

The upper half in Figure 3.1 is channel 1 of our system, and the lower half is channel 2. Each channel is an oscillator consisting of 5 adders, 6 multipliers, 1 divider, 2 integrators, 1 sine block, and 1 cosine block. We use scopes (not all shown in the figure) to display output data.

3.1.2 Simulation Results

Ideally, both channels should eventually oscillate at the same frequency, and their steady-state magnitude and phase difference should be the value determined by Equation 2.13 and 2.10. In Chapter 1 we have discussed that the oscillating frequency can be very low for the biological applications we care. Therefore here we choose ω_1 and ω_2 to be of the order of 1 rad/s. Setting K to be 2, ω_1 to be 1 rad/s, and ω_2 to be 2 rad/s, we get the results shown in Figure 3.2 and 3.3. It should be noted that the initial values of r_1, r_2, φ_1, and φ_2 do not affect the stable state results as long as those of r_1 and r_2 are not zero. Here they are set to be 2.0, 0.2, -6.3, and -5.3, respectively.

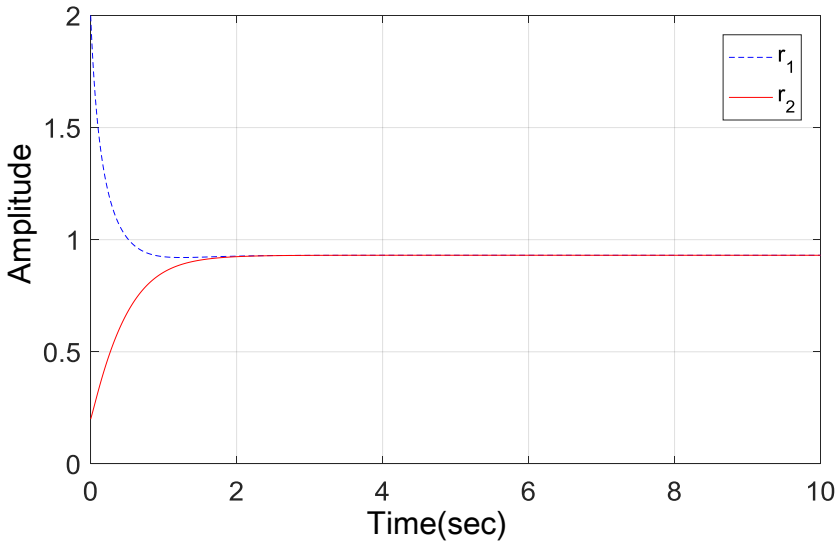

Figure 3.2: Time domain response of r_1 and r_2.

As we can see, after a few seconds, r_1 and r_2 converge to the same value, around 0.931, which is the same as the value calculated from Equation 2.13. Meanwhile, the

phase difference between the two channels becomes a constant value of 0.523 rad, which also agrees with Equation 2.10. Thus we conclude that the model described by Equation 2.5 does work.

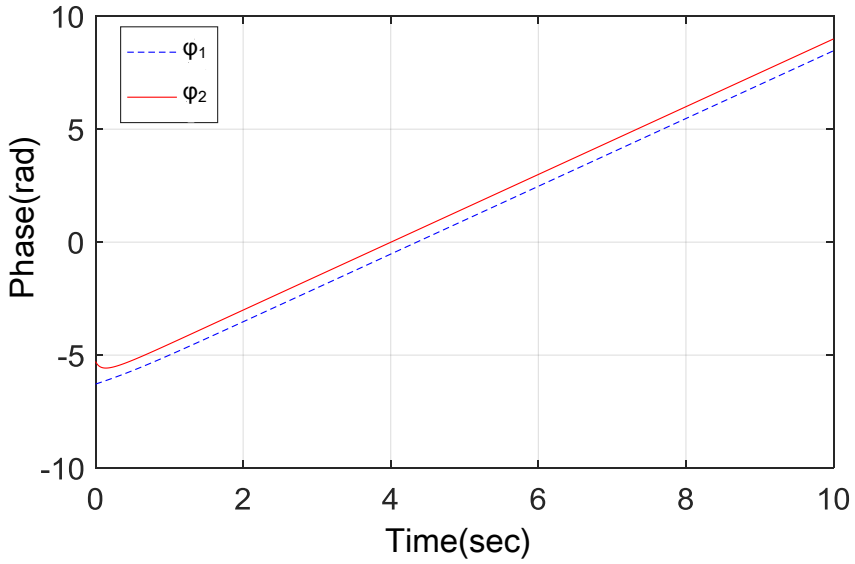

Figure 3.3: Time domain response of φ_1 and φ_2.

Since $x = r\cos\varphi,\ y = r\sin\varphi$, we can add a few more blocks (1 sine, 1 cosine, and 2 multipliers for each channel) to the system shown in Figure 3.1 to convert r and φ to x and y. The waveforms are shown in Figure 3.4, which are perfect sine waves as expected.

Another phenomenon we want to look at is how r changes with $\omega_2 - \omega_1$. In chapter 2, we already got the explicit expression 2.13. Here we fix ω_1 and K at 1 and 2, respectively. Then change ω_2 from 0.5 to 2.5. The results are shown in Figure 3.5. As expected, when ω_2 changes from 1.0(=ω_1) to 2.5, r decreases from 1.000 to 0.813. It should be noted that the two curves of $\omega_2 = 0.5$ and $\omega_2 = 1.5$

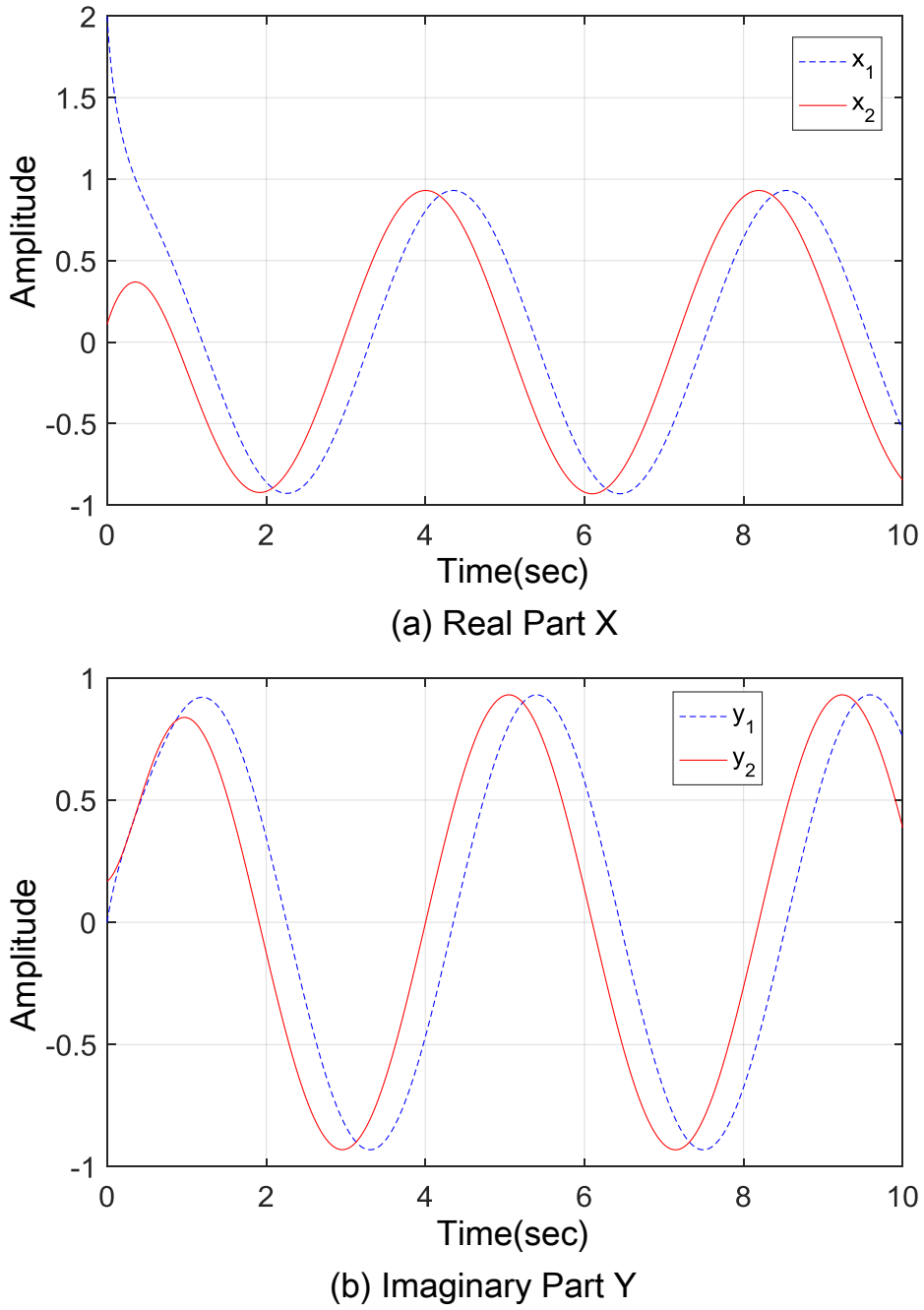

Figure 3.4: Time domain response of x and y.

overlap when the system becomes stable. This agrees with our discussion in chapter 2 that only the absolute value of $\omega_2 - \omega_1$ will affect the final value of r. But the relative phase between the two channels in these two cases will be swapped, as shown

in Figure 3.6.

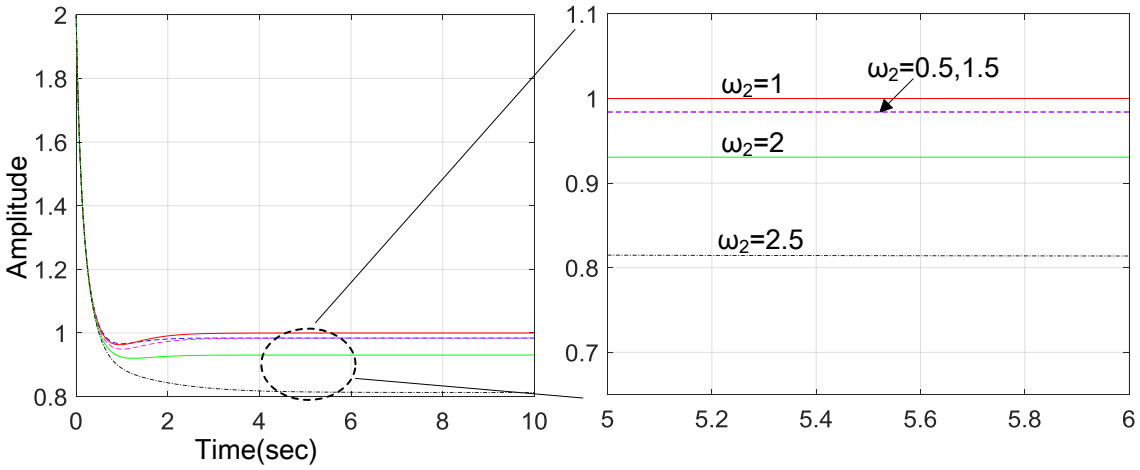

Figure 3.5: How r changes as ω_2 changes with $\omega_1 = 1$ and $K = 2$.

3.2 Implementation with Real and Imaginary Parts

3.2.1 System Modeling

Setting K to be 2, Equation 2.14 becomes:

$$\begin{aligned} \frac{dx_k}{dt} &= -\omega_k y_k - x_k(x_k^2 + y_k^2) + x_i \\ \frac{dy_k}{dt} &= \omega_k x_k - y_k(x_k^2 + y_k^2) + y_i \end{aligned} \tag{3.2}$$

where $k = 1, 2, i = 3 - k$. Similar to the previous section, we set up our oscillator system by replacing all mathematical operations in Equation 3.2 with their corresponding blocks in Simulink. The new oscillator system is shown in Figure 3.7. The left half is channel 1 and the right half is channel 2. Each channel consists of 6 multipliers, 5 adders, and 2 integrators.

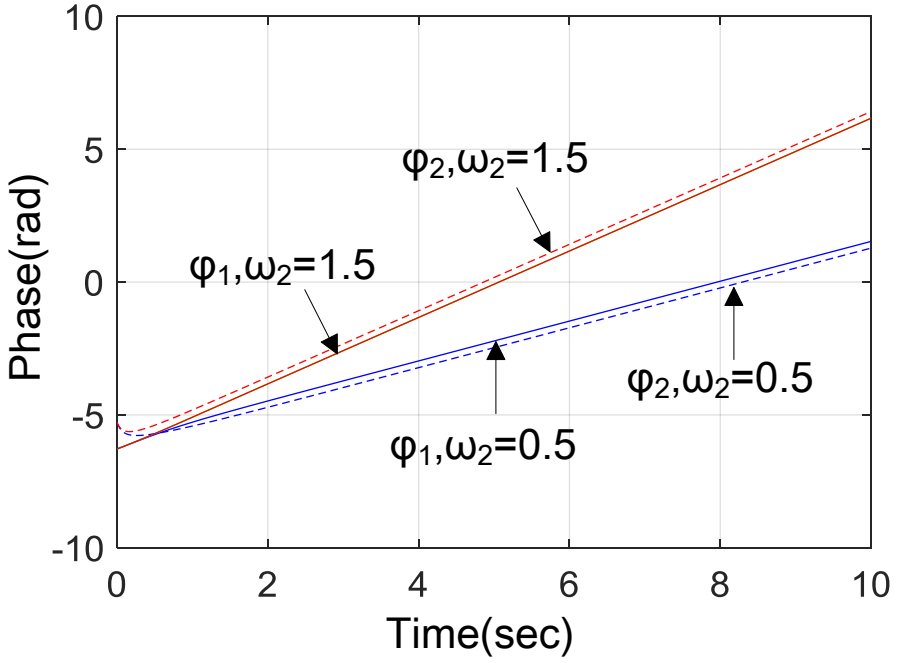

Figure 3.6: Time domain response of φ_1 and φ_2 for $\omega_2 = 0.5$ and 1.5, $K = 2$.

3.2.2 Simulation Results

Setting ω_1 and ω_2 to be 1 rad/s and 2 rad/s, respectively, simulation results are shown in Figure 3.8. For this new oscillator system, we get perfect sine waveforms in both channels. Comparing Figure 3.8 to Figure 3.4, we can see that both systems have the same time response when they become stable. This makes sense because they are dealing with exactly the same model. The only difference is how they approach it. One system deals with magnitude and phase while the other works with real part and imaginary part.

3.3 Chapter Summary

In this chapter we simulated two globally coupled oscillator systems in Simulink to verify the model proposed by Matthews et al.. Simulation results show that both systems work perfectly, and they have the same time response. This gives us a guidance for the next chapter, where we will design an globally coupled oscillator system with integrated circuits.

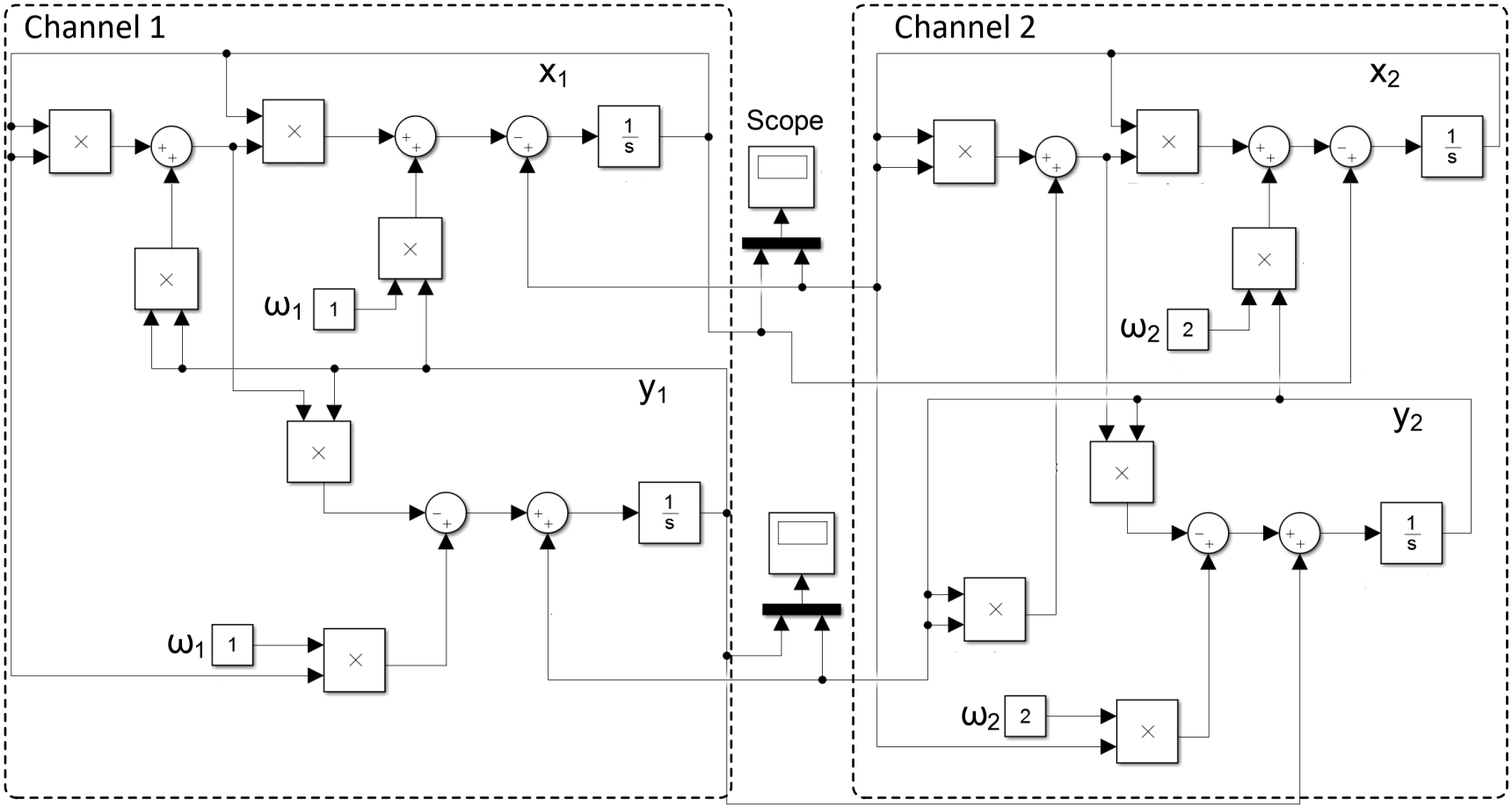

Figure 3.7: New oscillator system in Simulink.

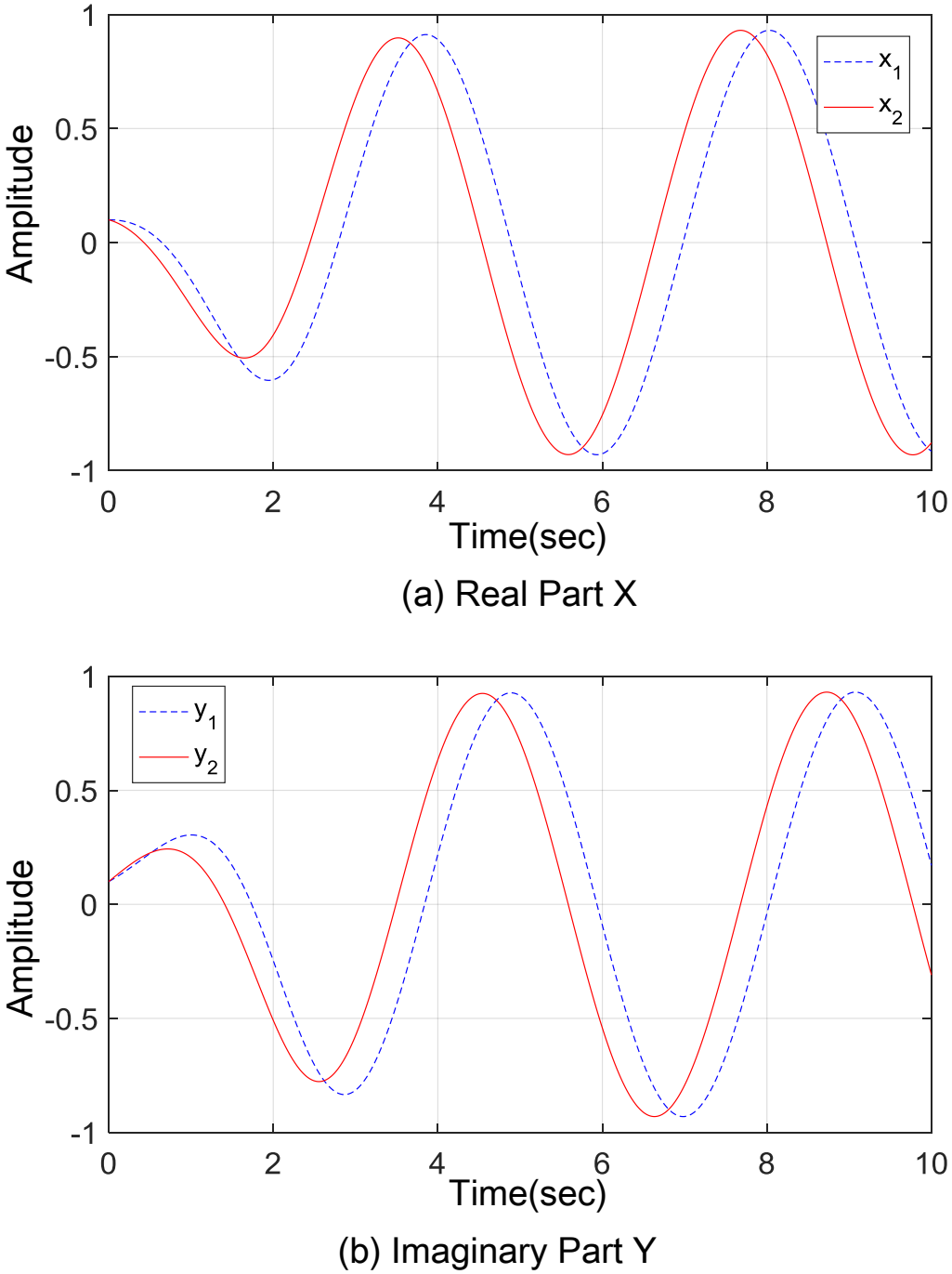

Figure 3.8: New time domain response of x and y.

Chapter 4: Oscillator System Design and Implementation with CMOS Circuits

The main purpose of this thesis is to design and simulate a globally coupled oscillator system based on the model proposed by Matthews et al. [59] using complementary metal-oxide-semiconductor (CMOS) circuits. From chapter 2 we can see that this involves the design of many subcircuits, including multipliers, operational transconductance amplifiers (OTAs), current mirrors and so on. In this chapter, we will discuss design techniques for these key components one by one. Most circuits work in above threshold. But some circuits, like transconductance amplifiers, need to work in subthreshold. In the end of this chapter, we will design the whole oscillator system and simulate it. We will also present simulation results.

4.1 Overall Specifications

The system we are dealing with is a two-channel globally coupled oscillator described by Equation 3.2. Table 4.1 shows specifications of our oscillator system.

Table 4.1: Specifications of our oscillator system

Parameter	Specification
Number of Channels	2
ω_1	1 rad/s
ω_2	2 rad/s
K	2
Technology	ON Semiconductor 0.5 μm CMOS
Supply Voltage	$\pm$5 V
Maximum Capacitance	1 nF

4.2 Subcircuit Design

4.2.1 Integrators

Designing the oscillator involves designing many subcircuits. Here we deal with integrators first because their implementation can significantly affect the requirements of other circuits. First, we look at the equations for one channel:

$$\begin{aligned} \frac{dx_1}{dt} &= -\omega_1 y_1 - x_1(x_1^2 + y_1^2) + x_2 \\ \frac{dy_1}{dt} &= \omega_1 x_1 - y_1(x_1^2 + y_1^2) + y_2. \end{aligned} \tag{4.1}$$

The time derivative of x_1 and y_1 is the sum of several signals. A brute force idea is just replacing each mathmatical operator by its corresponding analog circuit similar to what we did with Simulink. If this is the case, we need to work with analog

integrators. Most analog integrators make use of operational amplifiers and capacitors [68–73], as shown in Figure 4.1(a). In this circuit, we have:

$$\begin{aligned} i_c &= C\frac{dV_c}{dt} = C\frac{d(V_x - V_{out})}{dt} = -C\frac{dV_{out}}{dt} \\ i_c &= (V_{in} - V_x)/R = V_{in}/R \end{aligned} \tag{4.2}$$

which gives us:

$$V_{out}(t) = -\frac{1}{RC}\int_0^t V_{in}(t)dt + V_{out}(0). \tag{4.3}$$

By making a slight modification to the circuit in 4.1(a), we can get an integrator with multiple inputs, as shown in Figure 4.1(b). Then the relationship between the output and inputs is:

$$-C\frac{dV_{out}}{dt} = \frac{V_{in1}}{R_1} + \frac{V_{in2}}{R_2}. \tag{4.4}$$

By expanding the integrator circuit in Figure 4.1 in this way, we can achieve the summation described by Equation 4.1 and thus realize our whole oscillator system.

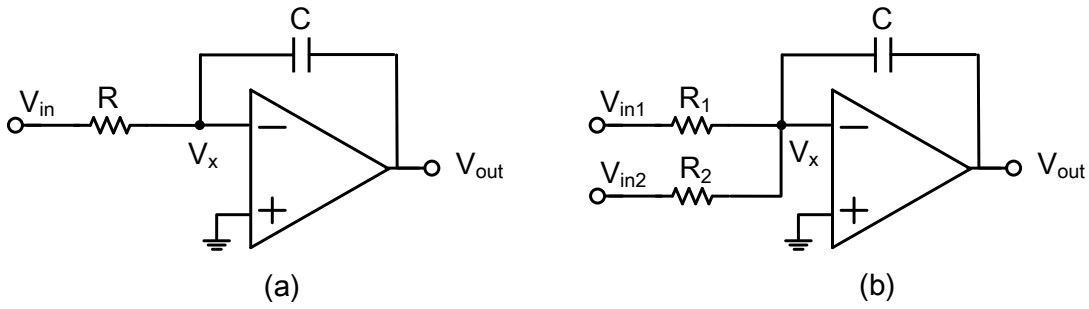

Figure 4.1: Typical continuous time integrator.

However, there are several problems if we use the above integrator. For an operational amplifier to work properly, the input must be within a certain range. Generally speaking, the input of an operational amplifier consists of two parts. The

first one is a common mode voltage which sets the DC operating point and thus insures its functionality and performance. The second one is a non-constant part, resulting in change at the output. Depending on its internal design, the allowed input range varies significantly. In our case, the input for one operational amplifier will be proportional to $-\omega_1 y_1 - x_1(x_1^2 + y_1^2) + x_2$, which increases linearly as ω_1 increases. Since we want our oscillator to work at different frequencies, the actual input range needed for operational amplifiers can be very large. Thus it will be very difficult to design the operational amplifier. On the other hand, an operational amplifier consists of several transistors to hundreds of transistors, depending on its performance requirement. Using an operational amplifier based integrator may make our oscillator circuit much more complicated than necessary.

Despite various implementations, the key component of integrators is the capacitor. For a linear constant capacitor, the following equation always holds true:

$$I_c = C\frac{dV_c}{dt} \tag{4.5}$$

In other words, if we use a single capacitor as an integrator, the circuit always works perfectly regardness of input value. Previously when we discussed operational amplifier based integrators, input signals were voltages. But for a single capacitor integrator, inputs are currents. This gives it another advantage since we can get the sum of currents by simply connecting multiple input currents to the same capacitor. No extra circuit is needed. The biggest challenge is that without an operational amplifier, inputs are connected to the capacitor directly, which means the capacitor

is a load for previous circuits. The capacitor voltage (one of x_1, y_1, x_2, and y_2) oscillates between $-r$ and r as time goes by, causing significant output voltage change in the circuit driving it. Consequently, all subcircuits including transconductance amplifiers, current mirrors, and multipliers have to work with a capacitive load at different voltage levels. This will make them much more difficult to realize. Considering all factors including circuit complexity, reliability and feasibility, we adopt single capacitor integrators without operational amplifiers in our design.

4.2.2 Wide Input Range Multipliers

Multipliers are an essential part in our oscillator system. A simple multiplier has two input ports and one output port. The input and output can be either voltage signals or current signals. The output is the product of the two input signals times a scaling factor. Depending on the polarity of the input signals, multipliers can be divided into 3 categories, as shown in Table 4.2. Here x and y stand for the two inputs, and z stands for the output signal. Unipolar signals are signals that swing from zero to positive full-scale, while bipolar signals are signals that swing from negative full-scale to positive full-scale. If both inputs are unipolar, the output is unipolar and this is a single quadrant multiplier. If one input is unipolar and the other is bipolar, the output is bipolar and it is a double quadrant multiplier. If both inputs are bipolar, the output is also bipolar and this multiplier is a four quadrant multiplier.

In our oscillator system, multipliers' inputs are differential voltages represent-

Table 4.2: Different multiplier types

x	y	z	Type
Unipolar	Unipolar	Unipolar	Single Quadrant
Bipolar	Unipolar	Bipolar	Double Quadrant
Unipolar	Bipolar	Bipolar	Double Quadrant
Bipolar	Bipolar	Bipolar	Four Quadrant

ing x_k and y_k, and their outputs are current signals charging and discharging capacitors. Simulation results in chapter 3 have shown that both channels' real and imaginary parts oscillate between $-r$ and r, with the value of r determined by K, ω_1, and ω_2. In other words, both inputs of the multiplier are bipolar signals varying between $-r$ and r. Thus we need a four quadrant transconductance multiplier with a wide input voltage range.

Since the 1950s, there has been a lot of research in four quadrant multipliers [74–82]. Before we discuss four quadrant multipliers, let us first review some basic knowledge of multipliers. Multipliers usually make use of some nonlinear device whose output is a polynomial of its input. Figure 4.2 shows the basic idea of multipliers [82]. Two input signals $v_1(t)$ and $v_2(t)$ are applied to the input, making up an equivalent input $v_i(t) = v_1(t) + v_2(t)$. This input signal goes into a nonlinear circuit and generates an output which consists of terms such as $v_1(t)$, $v_2(t)$, $v_1(t)v_2(t)$, $v_1(t)^2$, $v_2(t)^2$, and so on. Since we only need the $v_1(t)v_2(t)$ term, this output has to go through another circuit to cancel out unwanted terms like $v_1(t)^2$

and $v_2(t)^2$. After this nonlinearity cancellation circuit, the final output current is generated, and it is proportional to $v_1(t)v_2(t)$. Thus a simple multiplier is achieved.

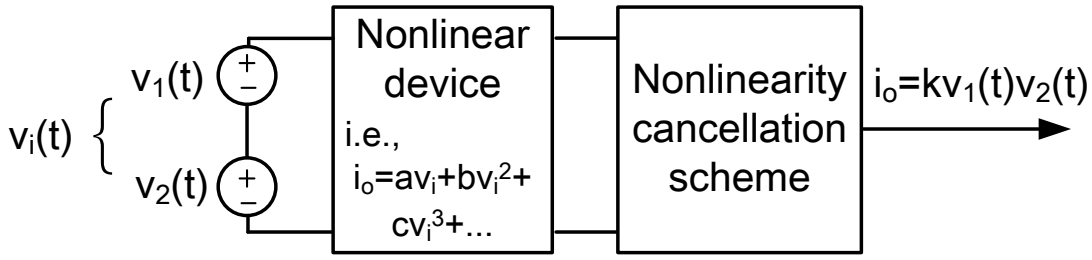

Figure 4.2: Basic idea of multipliers.

In [82], Han and Sanchez-Sinencio summarized two main methods for nonlinearity cancellation in four quadrant multipliers, as shown in Figure 4.3. Both circuits work with differential inputs and outputs. For simplicity, common mode voltages

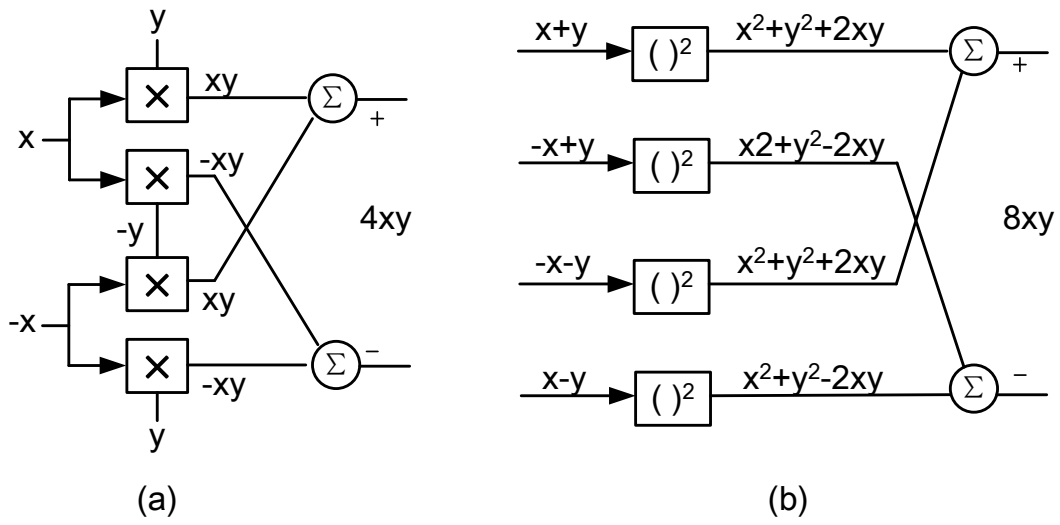

Figure 4.3: Four quadrant multiplier basic architectures. (a) Using single quadrant multipliers. (b) Using square devices.

are not shown. The first one makes use of single quadrant multipliers, while the second one adopts square devices. Let X and Y denote common mode voltages of the two inputs, respectively. Then for the first circuit in Figure 4.3, we have:

$$\begin{aligned} z &= ((X+x)(Y+y)+(X-x)(Y-y))-((X-x)(Y+y)+(X+x)(Y-y)) \\ &= (2XY+2xy)-(2XY-2xy) \\ &= 4xy \end{aligned} \tag{4.6}$$

Similarly, for the second circuit, we have:

$$\begin{aligned} z &= ((X+x+Y+y)^2+(X-x+Y-y)^2)-((X-x+Y+y)^2+(X+x+Y-y)^2) \\ &= 2((X+Y)^2+(x+y)^2)-2((X+Y)^2+(x-y)^2) \\ &= 2(x+y)^2-2(x-y)^2 \\ &= 8xy \end{aligned} \tag{4.7}$$

Thus both circuits do nonlinearity cancellation simultaneously with multiplication.

Although the two circuits in Figure 4.3 use different nonlinearity cancellation methods, both of them need nonlinear devices (Figure 4.3(a) uses single quadrant multipliers, which consist of nonlinear devices and other circuits). So we need some kind of device, or circuit, that has this polynomial property. Fortunately a MOSFET displays polynomial relationship between its output and input signals. A MOSFET is a four-terminal device with source (S), gate (G), drain (D), and body (B) terminals. Current will flow through a MOSFET when certain voltages are applied to its terminals. An n-type MOSFET has the following properties when working in the

ohmic region and saturation region respectively:

$$I_D = \mu_n C_{ox} \frac{W}{L}((V_{GS} - V_{TH})V_{DS} - \frac{1}{2}V_{DS}^2),$$
$$\text{if } V_{GS} > V_{TH}, V_{DS} < V_{GS} - V_{TH} \tag{4.8}$$

$$I_D = \frac{1}{2}\mu_n C_{ox} \frac{W}{L}(V_{GS} - V_{TH})^2,$$
$$\text{if } V_{GS} > V_{TH}, V_{DS} > V_{GS} - V_{TH} \tag{4.9}$$

where C_{ox} is the gate oxide capacitance per unit area, V_{TH} stands for threshold voltage, and μ_n represents the mobility of electrons [68]. W and L are the width and length of the transistor. Depending on different power and performance requirements, some multipliers use MOSFETs operating in the ohmic region and some others use them in the saturation region. Among various multiplier types, the Gilbert Cell [68] is a fundamental circuit that uses MOSFETs operating in the saturation region. Figure 4.4 shows a basic Gilbert multiplier. For all circuits in this thesis, the bulk of n-type MOSFETs is connected to the lowest potential in that circuit (Vss or GND), and the bulk of p-type MOSFETs is connected to Vdd.

For the Gilbert multiplier shown in Figure 4.4, all transistors are working in saturation and they are perfectly matched such that:

$$\begin{aligned} (\frac{W}{L})_1 &= (\frac{W}{L})_2 = (\frac{W}{L})_3 = (\frac{W}{L})_4 \\ (\frac{W}{L})_5 &= (\frac{W}{L})_6 \end{aligned} \tag{4.10}$$

The differential output current is:

$$I_o = I_{o1} - I_{o2} = (I_{D1} + I_{D3}) - (I_{D2} + I_{D4})$$

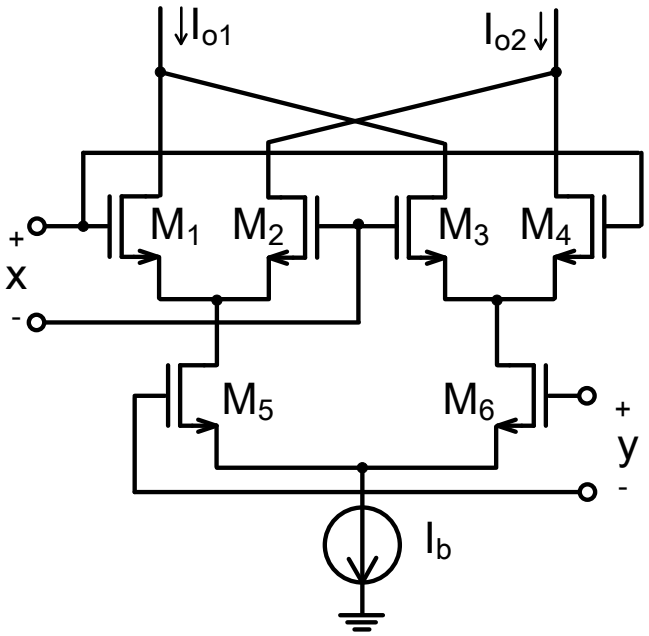

Figure 4.4: A MOS Gilbert multiplier.

To make equations more concise, do the following substitutions:

$$k_a = \mu_n C_{ox}(\frac{W}{L})_1$$
$$k_b = \mu_n C_{ox}(\frac{W}{L})_5. \tag{4.11}$$

The gate voltages of M_1 and M_2 are $\frac{x}{2}$ and $-\frac{x}{2}$ respectively. Since M_1 and M_2 are working in the saturation region, we have:

$$\begin{aligned} I_{D1} &= k_a(\frac{x}{2} - V_{S1})^2 \\ I_{D2} &= k_a(-\frac{x}{2} - V_{S1})^2 \end{aligned} \tag{4.12}$$

On the other hand, currents flowing through M_1 and M_2 also go through M_5:

$$I_{D1} + I_{D2} = I_{D5} \tag{4.13}$$

Plugging Equation 4.12 into Equation 4.13, we get:

$$V_{S1} = \sqrt{\frac{I_{D5}}{2k_a} - \frac{x^2}{4}} \tag{4.14}$$

Thus we can further get:

$$\begin{aligned} I_{D1} - I_{D2} &= k_a((\frac{x}{2} - V_{S1})^2 - (-\frac{x}{2} - V_{S1})^2) \\ &= -2k_a V_{S1} x \\ &= -2k_a x\sqrt{\frac{I_{D5}}{2k_a} - \frac{x^2}{4}} \\ &= -\sqrt{2k_a}x\sqrt{I_{D5}}\sqrt{1 - \frac{k_a x^2}{2I_{D5}}} \end{aligned} \tag{4.15}$$

Similarly, we get:

$$I_{D3} - I_{D4} = \sqrt{2k_a}x\sqrt{I_{D6}}\sqrt{1 - \frac{k_a x^2}{2I_{D6}}} \tag{4.16}$$

Thus we have:

$$\begin{aligned} I_o &= I_{D1} - I_{D2} + I_{D3} - I_{D4} \\ &= -\sqrt{2k_a}x(\sqrt{I_{D5}}\sqrt{1 - \frac{k_a x^2}{2I_{D5}}} - \sqrt{I_{D6}}\sqrt{1 - \frac{k_a x^2}{2I_{D6}}}). \end{aligned} \tag{4.17}$$

If

$$\frac{k_a x^2}{2I_{D5}} \ll 1 \text{ and } \frac{k_a x^2}{2I_{D6}} \ll 1 \tag{4.18}$$

Equation 4.17 can be simplified to:

$$I_o = -\sqrt{2k_a}x(\sqrt{I_{D5}} - \sqrt{I_{D6}}) \tag{4.19}$$

which shows that I_o is linearly proportional to input x. In Equation 4.19, we still have terms I_{D5} and I_{D6}, which are controlled by input y. Since transistors M_5 and

M_6 are in saturation, we have:

$$\begin{aligned} I_{D5} &= k_b(-\frac{y}{2} - V_{S5})^2 \\ I_{D6} &= k_b(\frac{y}{2} - V_{S5})^2 \end{aligned} \tag{4.20}$$

which gives us:

$$\sqrt{I_{D5}} - \sqrt{I_{D6}} = -\sqrt{k_b}y. \tag{4.21}$$

Plugging this into Equation 4.19:

$$I_o = \sqrt{2k_a k_b}xy. \tag{4.22}$$

As a result, the output current is the product of input x and y times a constant factor $\sqrt{2k_a k_b}$. A transconductance multiplier is achieved. But a big problem is that all transistors have to be in saturation and Equation 4.18 has to be satisfied, which limits the input range of this multiplier. In 1985, van Horn et al. [83] proposed a method to extend the input range of operational amplifiers, which was later applied to multipliers as well [84]. Figure 4.5(a) shows the attenuator with a level shifter presented in [84].

In Figure 4.5(a), transistor M_1 operates in the ohmic region and M_2 operates in the saturation region. Thus we have:

$$\begin{aligned} I_{D1} &= \mu_n C_{ox}(\frac{W}{L})_1((V_{dd} - V_i - V_{TH})(V_{dd} - V_{o1}) - \frac{1}{2}(V_{dd} - V_{o1})^2) \\ I_{D2} &= \frac{1}{2}\mu_n C_{ox}(\frac{W}{L})_2(V_{o1} - V_i - V_{TH})^2 \end{aligned} \tag{4.23}$$

which gives us:

$$V_{o1} = (1 - \sqrt{\frac{W_1 L_2}{W_1 L_2 + W_2 L_1}})(V_i - V_{dd} - V_{TH}) + V_{dd}. \tag{4.24}$$

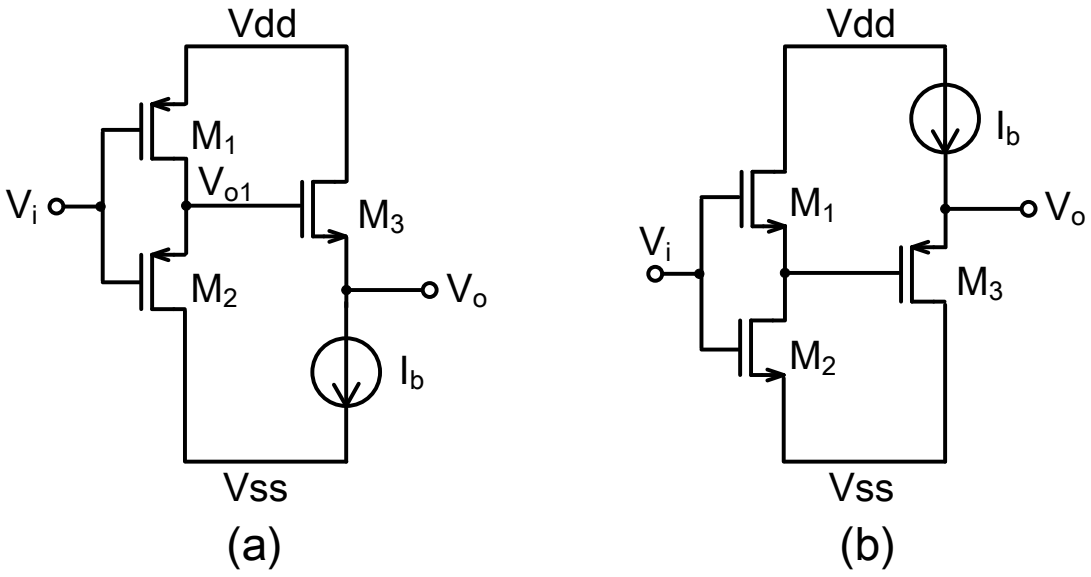

Figure 4.5: Attenuators. (a) Proposed by van Horn et al.. (b) Modified for our oscillator.

Thus the input amplitude is attenuated by a factor of $1-\sqrt{\frac{W_1L_2}{W_1L_2+W_2L_1}}$. As a result, a wider input range is allowed. The input pair M_1 and M_2 can also be n-type MOSFETS, as shown in Figure 4.5(b). Transistor M_3 is just a voltage follower. In Figure 4.5(a), it shifts down the voltage of V_{o1} by a certain level to insure proper common mode voltage for later circuits. We can replace M_3 with a p-type MOSFET if we want to shift up the voltage of V_{o1}, as shown in Figure 4.5(b).

Replacing the input stages of the multiplier proposed in [84] by the circuit shown in Figure 4.5(b), we get a multiplier for our oscillator system as shown in Figure 4.6. All transistors' sizes are presented in Appendix A. For the multiplier shown in Figure 4.6, wide input range differential inputs go through attenuators and generate signals with small AC amplitude. Then the generated signals go into a Gilbert cell. The output is a differential current $I_{op}-I_{on}$. A differential voltage

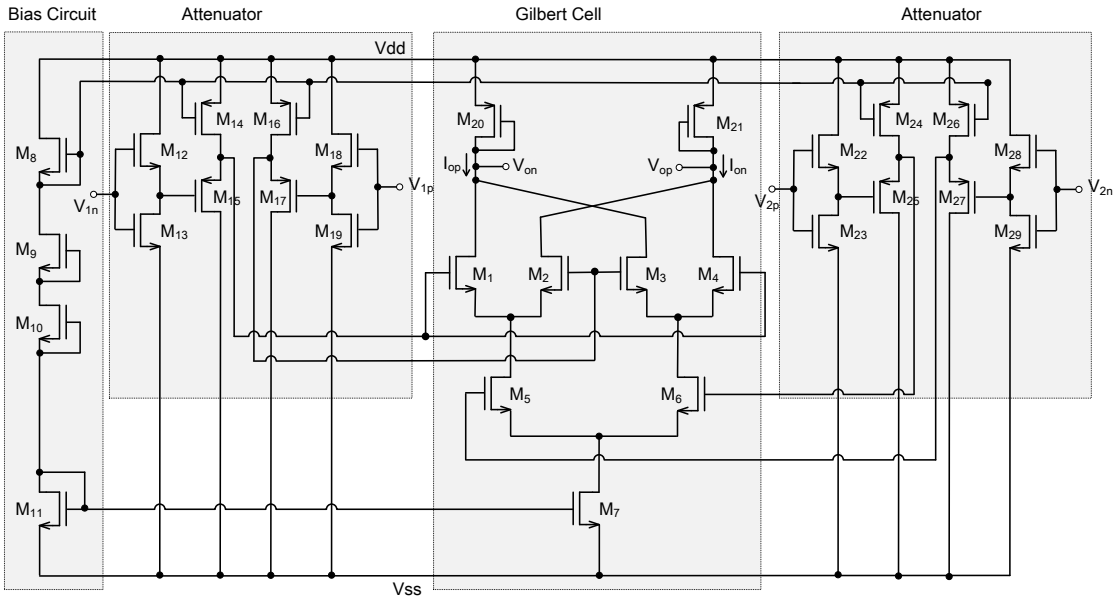

Figure 4.6: The multiplier for our oscillator.

output $V_{op} - V_{on}$ is generated by simply adding two transistors working as resistors.

4.2.3 Current Mirrors

Recall that to do integration, we need output currents from multipliers and transconductance amplifiers to charge and discharge capacitors. But for the multiplier shown in Figure 4.6, we cannot use the output currents I_{op} and I_{on} directly. The main reason is if we take these currents to charge capacitors, the functionality of this multiplier will be affected. So we need current mirrors to get another output current which can be used for charging and discharging. The same is also true for other subcircuits like transconductance amplifiers. Thus high linearity current mirrors capable of working with capacitive loads are demanded.

Figure 4.7(a) shows a basic current mirror using two transistors [85]. Both

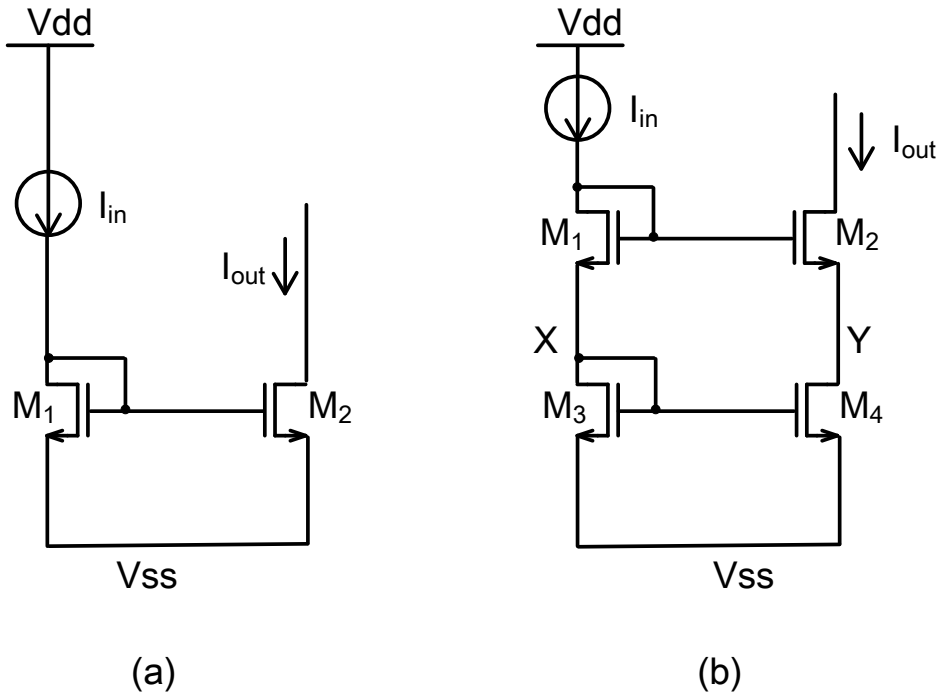

Figure 4.7: Current mirros. (a) Basic current mirror. (b) Cascode current mirror.

transistors work in the saturation region. The gate and drain terminals of transistor M_1 are tied together. Transistors M_1 and M_2 share the same gate voltage since their gates are connected. Thus we have:

$$\begin{aligned} I_{in} &= I_{D1} = \mu_n C_{ox}(\frac{W}{L})_1(V_{GS} - V_{TH})^2(1 + \lambda V_{DS1}) \\ I_{out} &= I_{D2} = \mu_n C_{ox}(\frac{W}{L})_2(V_{GS} - V_{TH})^2(1 + \lambda V_{DS2}) \end{aligned} \tag{4.25}$$

Ignoring body effect (set $\lambda = 0$) and cancelling out μ_n, C_{ox}, and $V_{GS} - V_{TH}$, we get:

$$I_{out} = \frac{(W/L)_2}{(W/L)_1} I_{in} \tag{4.26}$$

As a result, the output current is proportional to the input current. If transistors M_1 and M_2 have the same size and are both in saturation, the output current will

be an exact copy of the input current.

In reality, sometimes body effect cannot be ignored, especially when the current is very small. Then the actual output current is:

$$\frac{I_{out}}{I_{in}} = \frac{(W/L)_2}{(W/L)_1}\frac{1+\lambda V_{DS2}}{1+\lambda V_{DS1}}. \tag{4.27}$$

Since V_{DS2} might change as load changes, V_{DS1} and V_{DS2} are not guaranteed to be the same. Thus the linearity of this current mirror is seriously deteriorated. To overcome this, cascode current mirrors were introduced [85], as shown in Figure 4.7(b). In Figure 4.7(b), the DC voltages of V_Y and V_X are set to be the same. We can prove [68]:

$$\Delta V_Y \approx \Delta V_{out}/((g_{m2}+g_{mb2})r_{o2}). \tag{4.28}$$

Here Δ means the change in value. g_{m2} and g_{mb2} stand for the transconductance and backgate transconductance of M_2, respectively. From Equation 4.28 we can know that for the circuit shown in Figure 4.7(b), V_Y changes only slightly as output voltage changes. Thus V_Y can be regarded as equal to V_X and body effect is significantly reduced.

In our oscillator system, the output currents from multipliers and operational transconductance amplifiers are differential currents. We want to use them to charge and discharge capacitors. The bottom plates of capacitors are connected to ground to fix their voltages. Therefore only the upper plates are available for charging and discharging. Thus the outputs from multipliers and operational transconductance amplifiers need to be converted into single-ended signals. This can be achieved by adding another cascode current mirror composed of p-type transistors. Figure 4.8

shows the circuit of our current mirror.

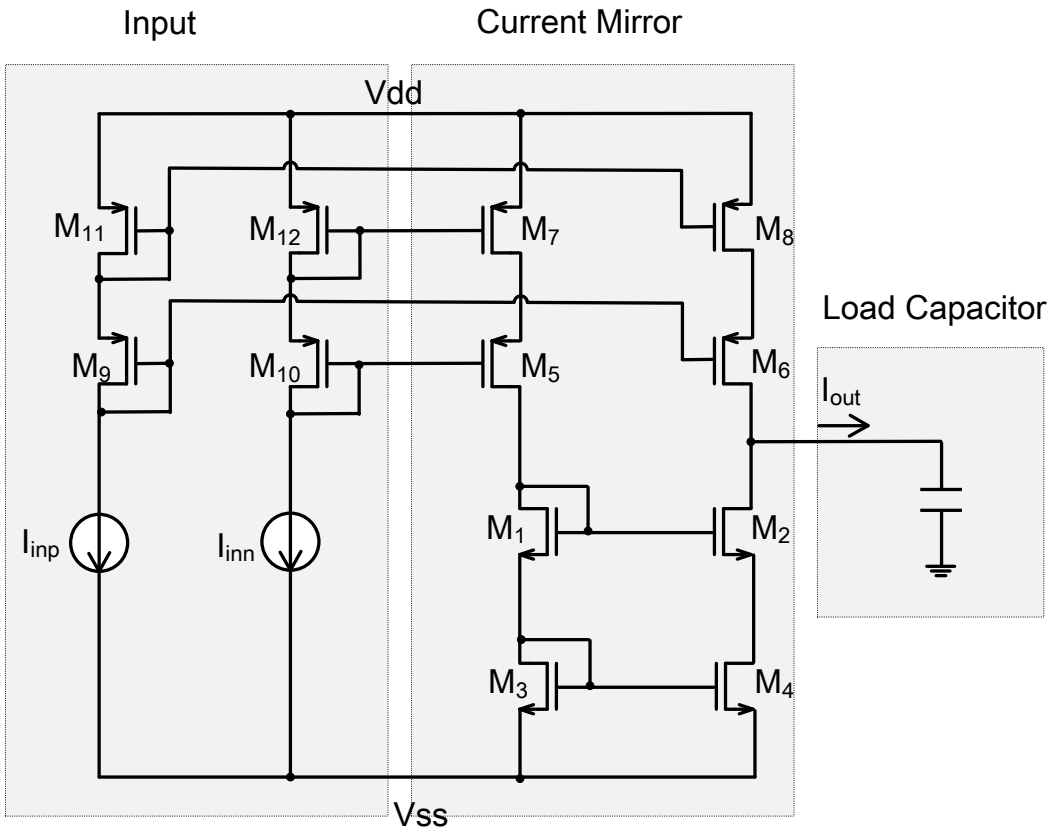

Figure 4.8: Current mirrors used in our circuit.

For the current mirror shown in Figure 4.8, I_{inp} and I_{inn} give the differential input current $I_{inp} - I_{inn}$. Using three cascode current mirrors, I_{D6} copies I_{inp} and I_{D2} copies I_{inn}. Current I_{D6} also flows through transistor M_2 and our load capacitor. Although we draw an arrow pointing to the capacitor, the actual output current can flow in both directions. When I_{out} is positive, the capacitor gets charged. And

if I_{out} is negative, the capacitor discharges. Thus we have:

$$\begin{aligned} I_{D6} &= I_{D9} = I_{inp} \\ I_{D5} &= I_{D10} = I_{inn} \\ I_{D2} &= I_{D1} = I_{D5} \\ I_{D6} &= I_{D2} + I_{out}. \end{aligned} \tag{4.29}$$

As a result:

$$I_{out} = I_{inp} - I_{inn}. \tag{4.30}$$

Note that the bottom plate of the capacitor is connected to ground. Thus the capacitor voltage stands for x_k or y_k in Equation 3.2. In previous chapters we have shown that this voltage will oscillate between $-r$ and r. Thus we need to guarantee that our current mirrors still work when the output voltage varies in this range. This is the reason why we choose cascode current mirrors over two-transistor current mirrors. Using cascode current mirrors, V_{D8} and V_{D4} stay almost constant regardless of the output voltage. Furthermore, we used $V_{ss} = -V_{dd}$ as negative rail to ensure all transistors are working in the saturation region.

Next we connect one multiplier and one current mirror together and run a simulation to see if they are working as expected. Figure 4.9 shows input and output waveforms when we set input voltages to be two sine waves with frequencies at 1 Hz and 7 Hz respectively. The two curves at the top are the two inputs. The curves at the bottom are the expected and actual output currents. As we can see, the actual output is so close to the expected output that they overlap and we can only see one curve. Both the multiplier and the current mirror are working perfectly

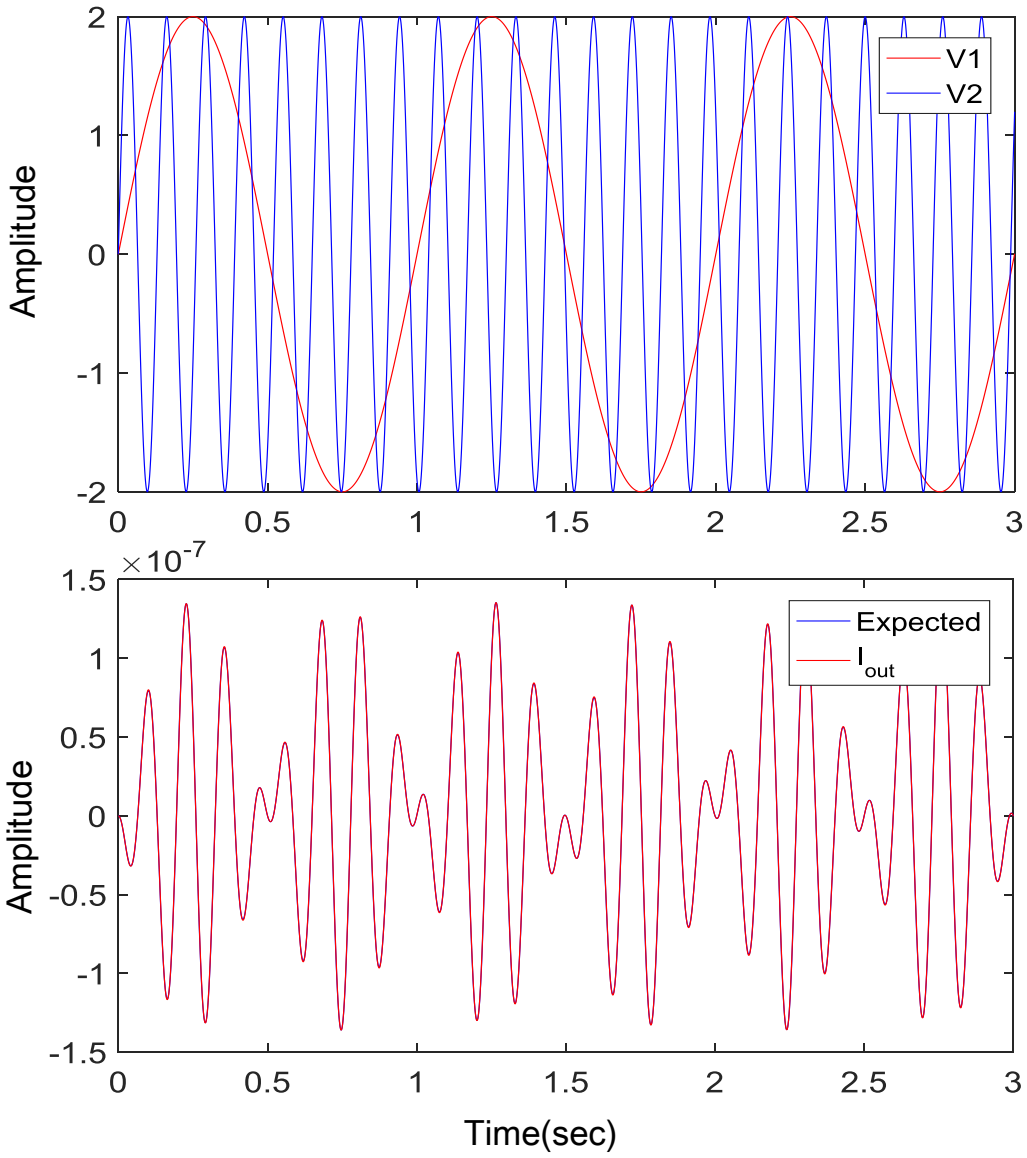

Figure 4.9: Output waveform of one multiplier connected to one current mirror.

with a 2-V input amplitude.

Another thing we want to check is the input range of our multiplier. Figure 4.10 shows the transfer characteristics of our multiplier. When carrying out this experiment, one terminal of each input is connected to ground and the actual input

is applied to the other terminal [84]. We set V_1 to be a ramp signal increasing from -4 V to 4 V and do a parameter sweep on V_2. As we can see, our multiplier works well for a very wide input range. Furthermore, simulation results in Chapter 3 have shown that x_k or y_k will not exceed ± 1 V. Therefore, we only care about the multiplier's performance when both inputs are within ± 1 V. As shown in Figure 4.11, the multiplier achieves very good linearity in this input range.

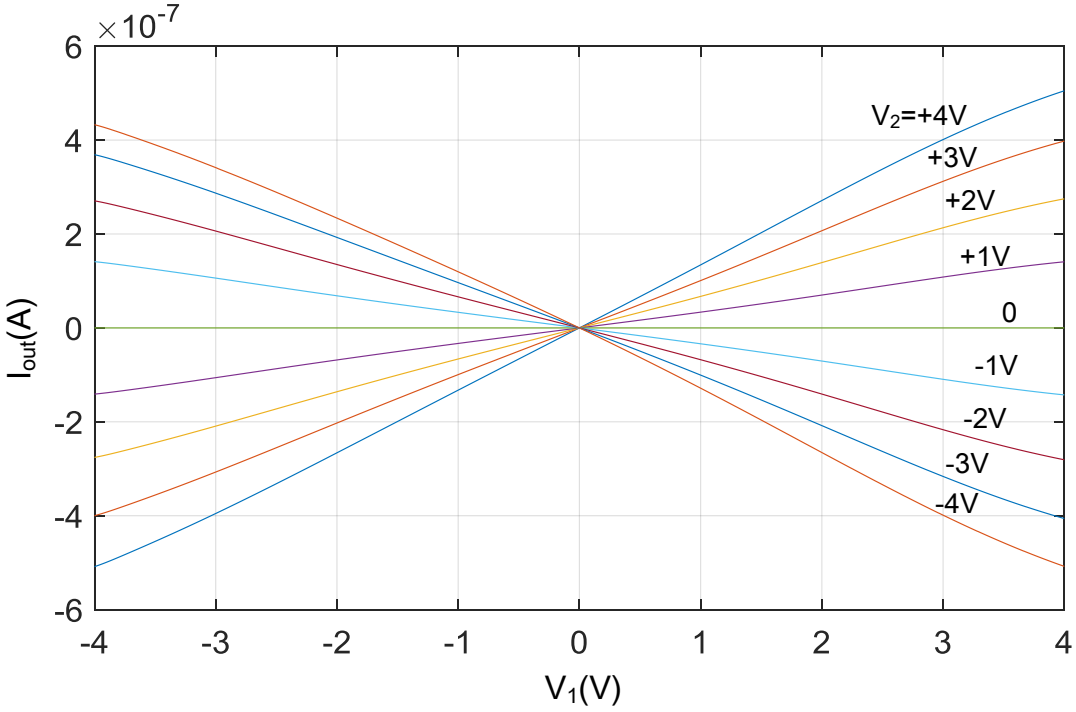

Figure 4.10: Transfer characteristics of our multiplier.

4.2.4 Operational Transconductance Amplifiers

Operational amplifiers are important components in applications such as integrators, differentiators, analog-to-digital converters, and so on. Figure 4.12(a) shows

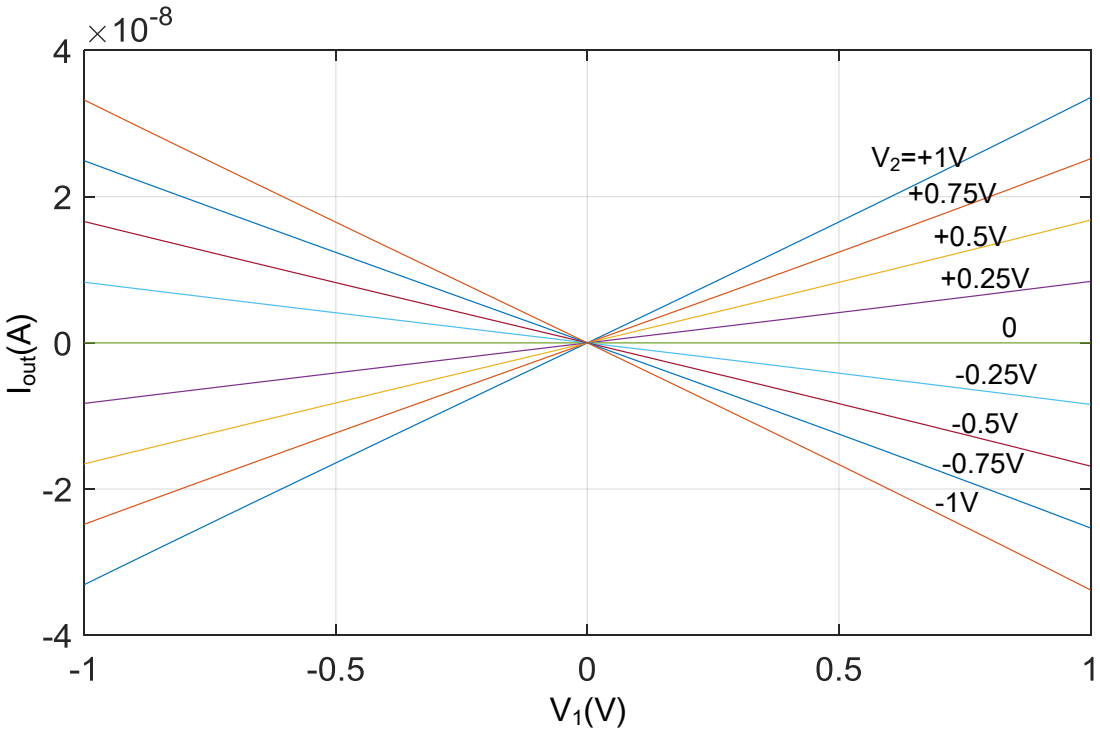

Figure 4.11: Transfer characteristics for inputs in [-1,1].

a schematic symbol for standard operational amplifiers. Both input and output are voltage signals, we have:

$$V_{out} = A(V_{in+} - V_{in-}) \tag{4.31}$$

where A stands for the open-loop voltage gain of this amplifier. An ideal operational amplifier has infinite voltage gain, infinite input resistance, and zero output resistance. In reality, A cannot be infinitely large, but can potentially vary from 10^2 to the order of 10^6. A tiny change at the input will cause a huge change, or even saturation, at the output. Thus depending on different application requirements, operational amplifiers may be used in either open-loop or closed-loop configurations, as shown in Figure 4.13. For simplicity, here we did not draw pins Vdd and Vss. In

Figure 4.13(b), the closed loop voltage gain is $1 + R_f/R_1$. By choosing appropriate values for R_f and R_1, we can guarantee that the output will not get saturated for a given input range.

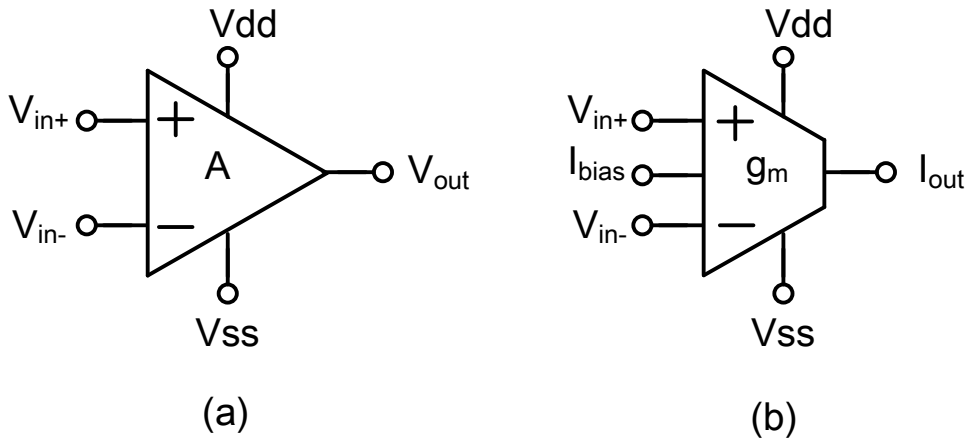

Figure 4.12: Schematic symbol for: (a) an op-amp (b) an OTA.

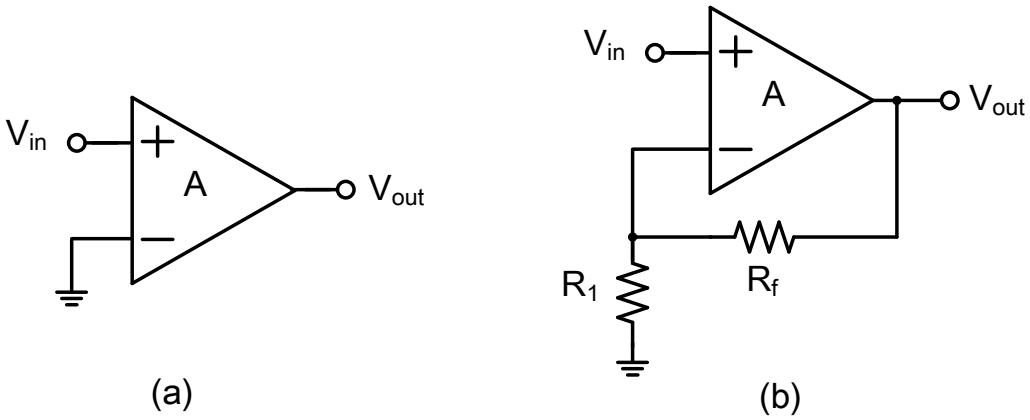

Figure 4.13: Open-loop and closed-loop applications of operational amplifiers. (a) Comparator. (b) Non-inverting amplifier.

Operational transconductance amplifiers are similar to standard operational amplifiers. The main difference is that now the output is a current signal, as shown

in Figure 4.12(b). For an operational transconductance amplifier, we have:

$$I_{out} = g_m(V_{in+} - V_{in-}) \tag{4.32}$$

where g_m stands for the transconductance of this amplifier. Usually, g_m can be directly controlled by I_{bias}. An ideal OTA has infinite input resistance and infinite output resistance. The output voltage depends on both output current and load resistance. Therefore, by choosing an appropriate value for load resistance, the amplifier can work in the open-loop configuration and its output will not get saturated. As a matter of fact, most transconductance operational amplifiers are used in open-loop, which is another difference from standard operational amplifiers.

Recall that a MOSFET working in the saturation region can be regarded as a voltage controlled current source. For an nMOS, if $\mathrm{V_{GS}} > \mathrm{V_{TH}}$ and $\mathrm{V_{DS}} > \mathrm{V_{GS}} - \mathrm{V_{TH}}$, the following equation holds true:

$$I_D = \frac{1}{2}\mu_n C_{ox}\frac{W}{L}(V_{GS} - V_{TH})^2 \tag{4.33}$$

Therefore, we can get its equivalent transconductance:

$$g_m = \frac{dI_D}{dV_{GS}} = \mu_n C_{ox}\frac{W}{L}(V_{GS} - V_{TH}) \tag{4.34}$$

Thus it seems straight forward to use two MOSFETs working in this region to build a differential transconductance amplifier, as shown in Figure 4.14. Here $\mathrm{M_1}$ and $\mathrm{M_2}$ are input transistors and they are perfectly matched ($\mathrm{W_1 = W_2, L_1 = L_2}$). $\mathrm{M_3}$ and

M_4 are also matched and they form a current mirror. Thus we have:

$$\begin{aligned} I_{out} &= I_{D4} - I_{D2} = I_{D1} - I_{D2} \\ g_{m1} &= g_{m2} = g_m \\ I_D &= g_m(V_{GS} - V_{TH}) \end{aligned} \tag{4.35}$$

As a result, the output current is:

$$I_{out} = g_m(V_{GS1} - V_{GS2}) = g_m(V_{inp} - V_{inn}) \tag{4.36}$$

The overall transconductance g_m of this amplifier is the same as the transconductance of M_1 and M_2.

However, the above circuit does not work for our oscillator system. Recall the equations that describe our oscillator system are:

$$\begin{aligned} \frac{dx_k}{dt} &= -\omega_k y_k - x_k(x_k^2 + y_k^2) + x_i \\ \frac{dy_k}{dt} &= \omega_k x_k - y_k(x_k^2 + y_k^2) + y_i. \end{aligned} \tag{4.37}$$

Here $k = 1, 2, i = 3 - k$. Since we use capacitor voltages to represent x_k and y_k, their time derivative stands for the current flowing through the capacitors. Thus we have:

$$\begin{aligned} I_{x_k} &= C\frac{dx_k}{dt} = -C\omega_k y_k - Cx_k(x_k^2 + y_k^2) + Cx_i \\ I_{y_k} &= C\frac{dy_k}{dt} = C\omega_k x_k - Cy_k(x_k^2 + y_k^2) + Cy_i. \end{aligned} \tag{4.38}$$

We want to use transconductance amplifiers to get terms such as $C\omega_1 y_k$ and Cx_i. Large capacitors occupy huge area and generate significant current which causes

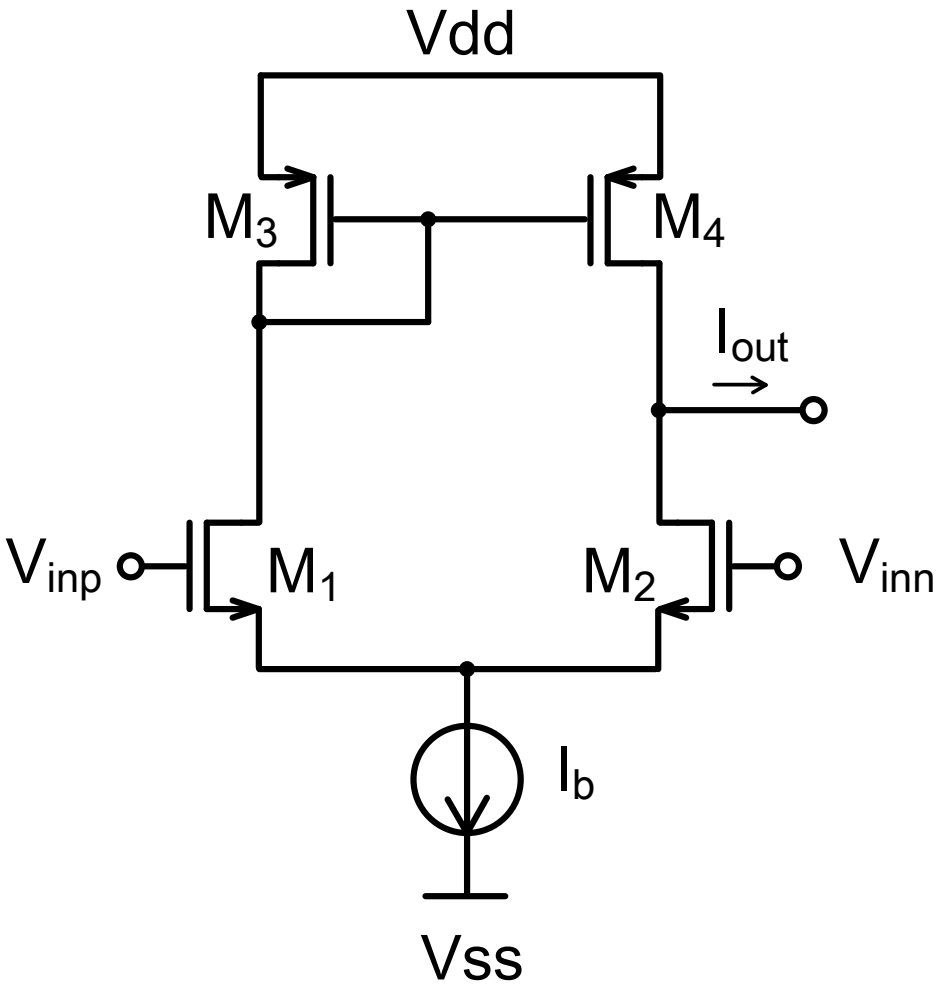

Figure 4.14: Schematic of a transconductance amplifier.

large power consumption. Therefore, we need to avoid using large capacitors. In this system, the maximum capacitor we are allowing to use is 1nF. That means the transconductance we expect is of the order of 10^{-9} A/V. Equation 4.34 gives us a way to estimate g_m. For the $0.5\mu m$ CMOS technology we use, a typical value for $\mu_n C_{ox}$ is 100 $\mu A/V^2$. $V_{GS}-V_{TH}$ can vary between 0.1V to several Volts. To achieve a transconductance of the order of 10^{-9} A/V, the transistor's aspect ratio W/L needs

to be of the order of 10^{-4} or smaller. Such a small aspect ratio is extremely difficult to match in layout [86]. In addition, the length of transistors would become very large. Such a transconductance amplifier is impractical for our system. Therefore, we need another transconductance amplifier circuit that is feasible.

Until now we only discussed how MOSFETs work when V_{GS} is larger than V_{TH}. Actually, when $V_{GS} < V_{TH}$, the transistor is not totally 'off'. There is still some current flowing through it, although quite small. We call this region the subthreshold region [85]. When an nMOS is working in subthreshold, its current is:

$$I_D = I_0 e^{\frac{\kappa V_{GB} - V_{SB}}{V_T}} (1 - e^{-\frac{V_{DS}}{V_T}}). \tag{4.39}$$

Here I_0 is determined by technology related parameters as well as transistor size. V_T is thermal voltage:

$$V_T = \frac{k_B T}{q} \tag{4.40}$$

where k_B is the Boltzmann's constant, T is the absolute temperature, and q is the magnitude of the electrical charge on the electron. κ is determined by:

$$\kappa = \frac{C_{ox}}{C_{ox} + C_j} \tag{4.41}$$

where C_j and C_{ox} stand for the depletion region capacitance and the gate oxide capacitance per unit area, respectively. If $V_{DS} > 4V_T$, we can get:

$$e^{-\frac{V_{DS}}{V_T}} \ll 1. \tag{4.42}$$

Thus Equation 4.39 can be simplified as:

$$I_D = I_0 e^{\frac{\kappa V_{GB} - V_{SB}}{V_T}}. \tag{4.43}$$

We call this region ($V_{GS} < V_{TH}, V_{DS} > 4V_T$) the saturation region for subthreshold operation. Now let us look at how the circuit in Figure 4.14 behaves if all transistors are working in subthreshold and saturation. Let V_S denote the voltage at the source of M_1 and M_2. We have:

$$\begin{aligned} I_{D1} &= I_0 e^{\frac{\kappa V_{inp} - V_S}{V_T}} \\ I_{D2} &= I_0 e^{\frac{\kappa V_{inn} - V_S}{V_T}} \end{aligned} \tag{4.44}$$

On the other hand, $I_{D1} + I_{D2} = I_b$, which gives us:

$$I_0(e^{\frac{\kappa V_{inp} - V_S}{V_T}} + e^{\frac{\kappa V_{inn} - V_S}{V_T}}) = I_b. \tag{4.45}$$

Solving this equation for V_S, we get:

$$e^{-\frac{V_S}{V_T}} = \frac{I_b}{I_0(e^{\frac{\kappa V_{inp}}{V_T}} + e^{\frac{\kappa V_{inn}}{V_T}})}. \tag{4.46}$$

Thus we can get the current for M_1 and M_2:

$$\begin{aligned} I_{D1} &= I_0 e^{\frac{\kappa V_{inp}}{V_T}} e^{-\frac{V_S}{VT}} = I_b \frac{e^{\frac{\kappa V_{inp}}{V_T}}}{e^{\frac{\kappa V_{inp}}{V_T}} + e^{\frac{\kappa V_{inn}}{V_T}}} \\ I_{D2} &= I_0 e^{\frac{\kappa V_{inn}}{V_T}} e^{-\frac{V_S}{VT}} = I_b \frac{e^{\frac{\kappa V_{inn}}{V_T}}}{e^{\frac{\kappa V_{inp}}{V_T}} + e^{\frac{\kappa V_{inn}}{V_T}}}. \end{aligned} \tag{4.47}$$

If the current mirror is still working, then the output current is:

$$\begin{aligned} I_{out} &= I_{D1} - I_{D2} = I_b \frac{e^{\frac{\kappa V_{inp}}{V_T}} - e^{\frac{\kappa V_{inn}}{V_T}}}{e^{\frac{\kappa V_{inp}}{V_T}} + e^{\frac{\kappa V_{inn}}{V_T}}} \\ &= I_b \tanh(\frac{\kappa}{2V_T}(V_{inp} - V_{inn})). \end{aligned} \tag{4.48}$$

The Taylor series expressions of hyperbolic tangent function is:

$$\tanh(x) = x - \frac{x^3}{3} + \frac{2x^5}{15} - \frac{17x^7}{315} + ... \tag{4.49}$$

If x is very small, higher order terms can be ignored:

$$\tanh(x) \approx x. \tag{4.50}$$

Thus if the differential input voltage is very small, the output current is:

$$I_{out} \approx \frac{\kappa I_b}{2V_T}(V_{inp} - V_{inn}). \tag{4.51}$$

Equation 4.51 shows that the output current is linearly proportional to the input voltage, which means that the circuit shown in Figure 4.14 does work as a transconductance amplifier in subthreshold. Furthermore, the transconductance is given by:

$$g_m = \frac{\kappa I_b}{2V_T}. \tag{4.52}$$

Therefore, the transconductance can be directly controlled by the bias current.

In figuring out the output current for the above transconductance amplifier in subthreshold, we assumed that M_3 and M_4 still work as a current mirror. Now, we will verify that they do. In subthreshold, we have:

$$\begin{aligned} I_{D3} &= I_{03} e^{\frac{\kappa V_{BG3} - V_{BS3}}{V_T}} (1 - e^{-\frac{V_{SD3}}{V_T}}) \\ I_{D4} &= I_{04} e^{\frac{\kappa V_{BG4} - V_{BS4}}{V_T}} (1 - e^{-\frac{V_{SD4}}{V_T}}). \end{aligned} \tag{4.53}$$

M_3 and M_4 are matched, and their gates are connected together. Also, their sources are both connected to Vdd. If they are working in saturation, we have:

$$I_{D3} = I_{03} e^{\frac{\kappa V_{BG3}}{V_T}} = I_{04} e^{\frac{\kappa V_{BG4}}{V_T}} = I_{D4} \tag{4.54}$$

which verifies that M_3 and M_4 do work as a current mirror in the subthreshold region. Therefore, the circuit shown in Figure 4.14 works as a transconductance

amplifier in the subthreshold region, provided that transistors are matched and in saturation. Making some modification to this circuit, we get a transconductance amplifier for our oscillator system, as shown in Figure 4.15. All transistors' sizes are presented in Appendix A.

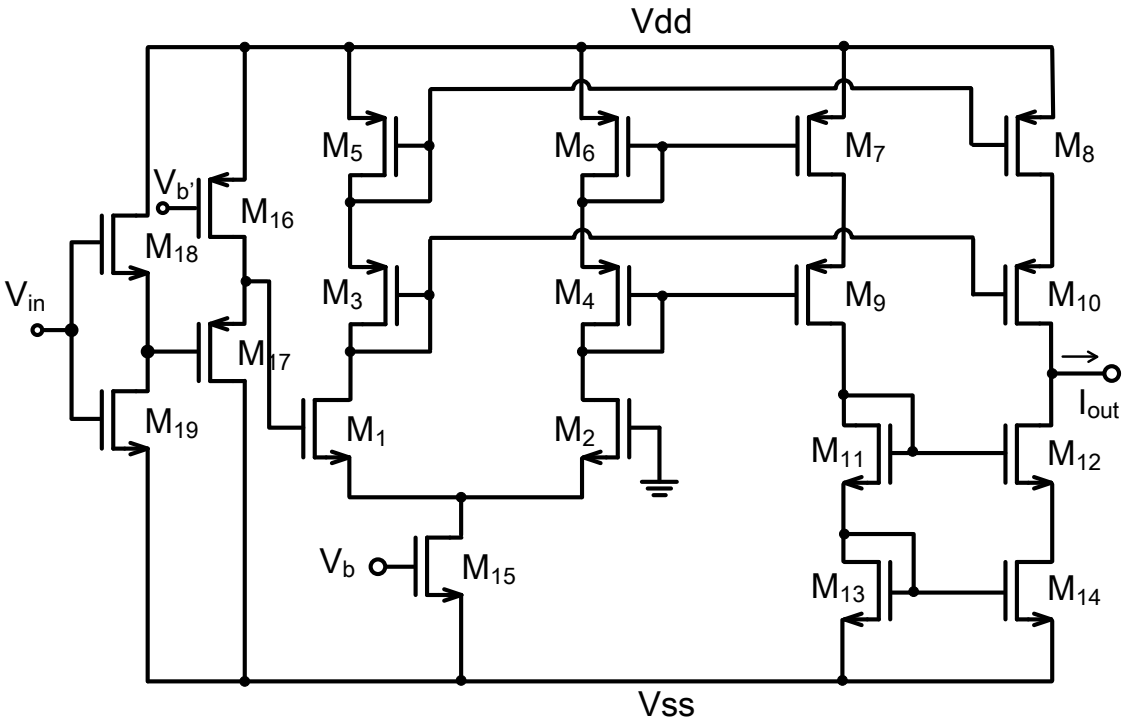

Figure 4.15: Schematic of transconductance amplifiers.

For the transconductance amplifier shown in Figure 4.15, M_{16} through M_{19} form an input stage. The transconductance amplifier's input voltage is in the range of $[-r, r]$, which is beyond the ohmic region of our hyperbolic tangent function approximation. Thus an attenuator is needed (M_{18} and M_{19}). We just reuse the attenuator circuit in Figure 4.5(b). The input is single-ended, so we simply connect the gate of M_2 to ground. As a result, we need a level shifter (M_{16} and M_{17}) to

guarantee a zero voltage at the gate of M_1 when the input is zero. M_3 through M_{14} form three current mirrors to get the output current. To control bias current, we used a voltage V_b to set the gate voltage of M_{15}. In other words, the transconductance of this amplifier can be easily set by setting different values for V_b.

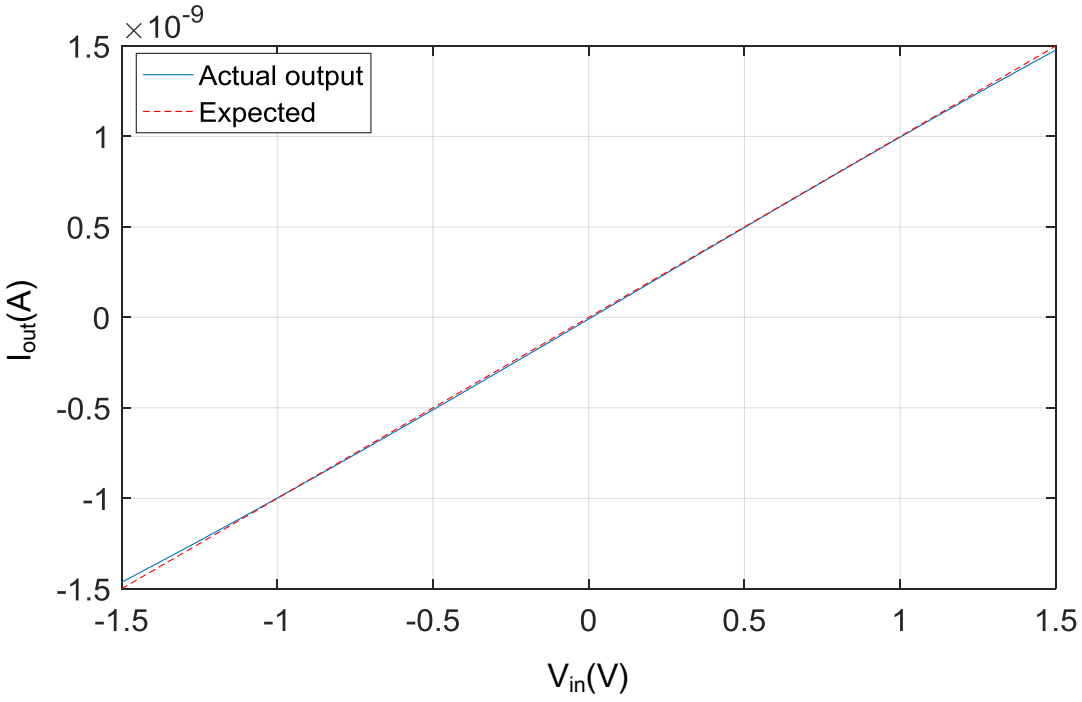

Figure 4.16: Transfer characteristic curve of our transconductance amplifier.

Figure 4.16 shows the transfer characteristic curve of our transconductance amplifier. As we can see, the actual output current matches well with the expected one, especially when the input voltage is in the range of $[-1, 1]$. In our oscillator system, the input voltage range for the transconductance amplifier is $[-r, r]$, with $r < 1$. In this range, our transconductance amplifier achieves very good linearity.

4.3 A Two-Channel Globally Coupled Oscillator System

4.3.1 Circuit Implementation

In previous sections, we have discussed the design of integrators, multipliers, current mirrors, and transconductance amplifiers. Using these circuits, we can build our two-channel globally coupled oscillator system, as shown in Figure 4.17. Here we only present one channel. The other channel is implemented in exactly the same way as this one, with different bias voltages for transconductance amplifiers to guarantee different transconductance values. As shown in Figure 4.17, the transconductance values are determined by C and oscillating frequency:

$$\begin{aligned} g_{m10} &= C\omega_1 \\ g_{m20} &= C\omega_2 \\ g_{m11} &= g_{m21} = C \end{aligned} \tag{4.55}$$

where g_{m20} and g_{m21} stand for corresponding transconductance values of the other channel. By setting different values for g_{m10} and g_{m20}, the system can oscillate at different frequencies.

In Figure 4.17, both capacitors have the same value of 1 nF. One capacitor voltage stands for x_1 and the other stands for y_1. We draw some arrows to indicate whether there is current flowing through a connection. The direction of the arrow does not matter. Current can flow in the opposite direction, too. The frequencies we work with are quite low (of the order of 0.1 rad/s to 10 rad/s). Thus no current will flow into or out of the inputs of multipliers and transconductance amplifiers

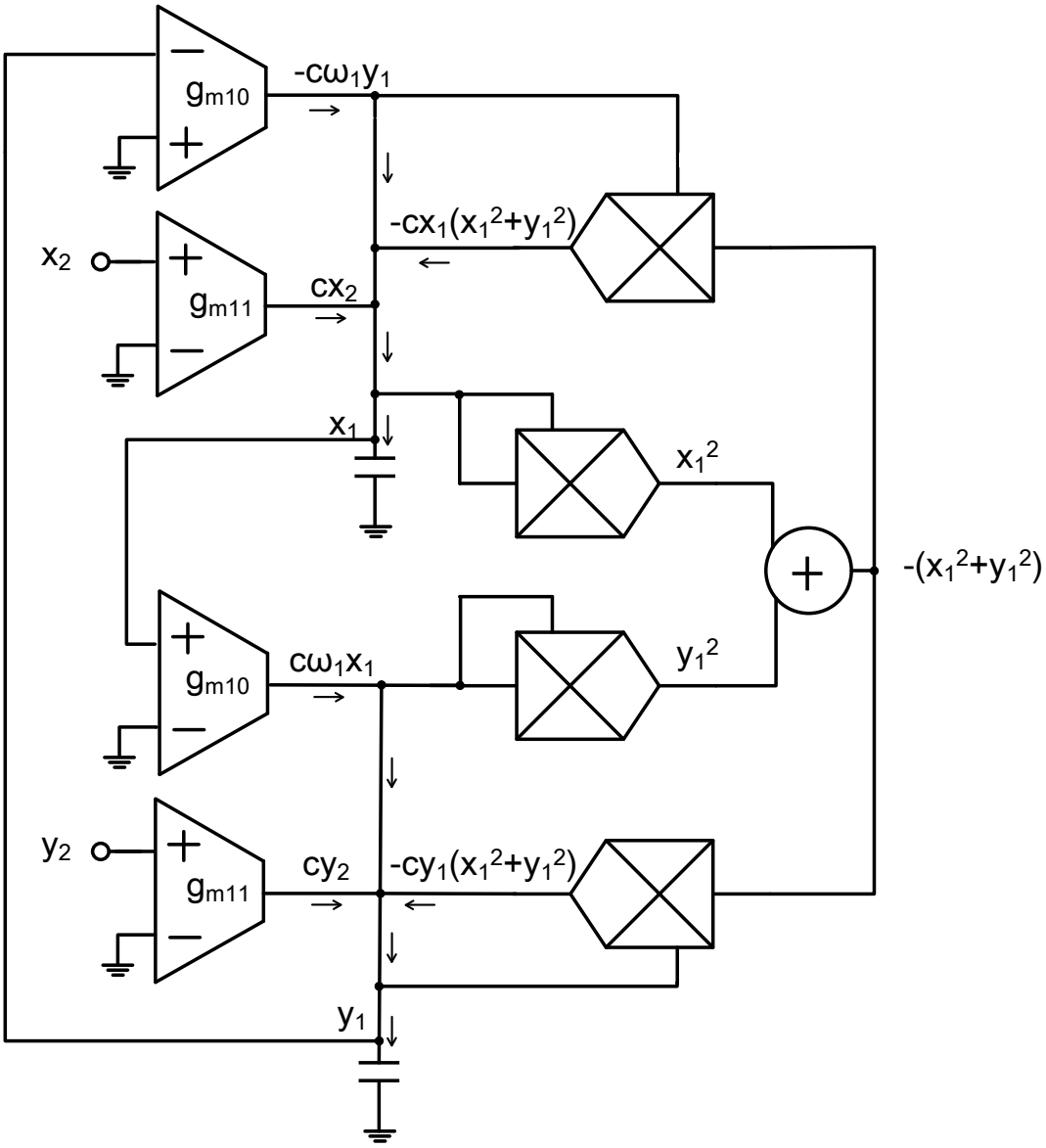

Figure 4.17: One channel of the oscillator.

although they are connected to the upper plates of capacitors.

4.3.2 Simulation Results

Setting up the full coupled oscillator system with $\omega_1 = 1$ rad/s and $\omega_2 = 2$ rad/s, we get the time domain response shown in Figure 4.18. As can be seen from the

figure, our circuit does work as an oscillator and it becomes stable after less than 1 cycle. When the system becomes stable, both channels are oscillating at the same frequency and amplitude and there is fixed phase difference between them.

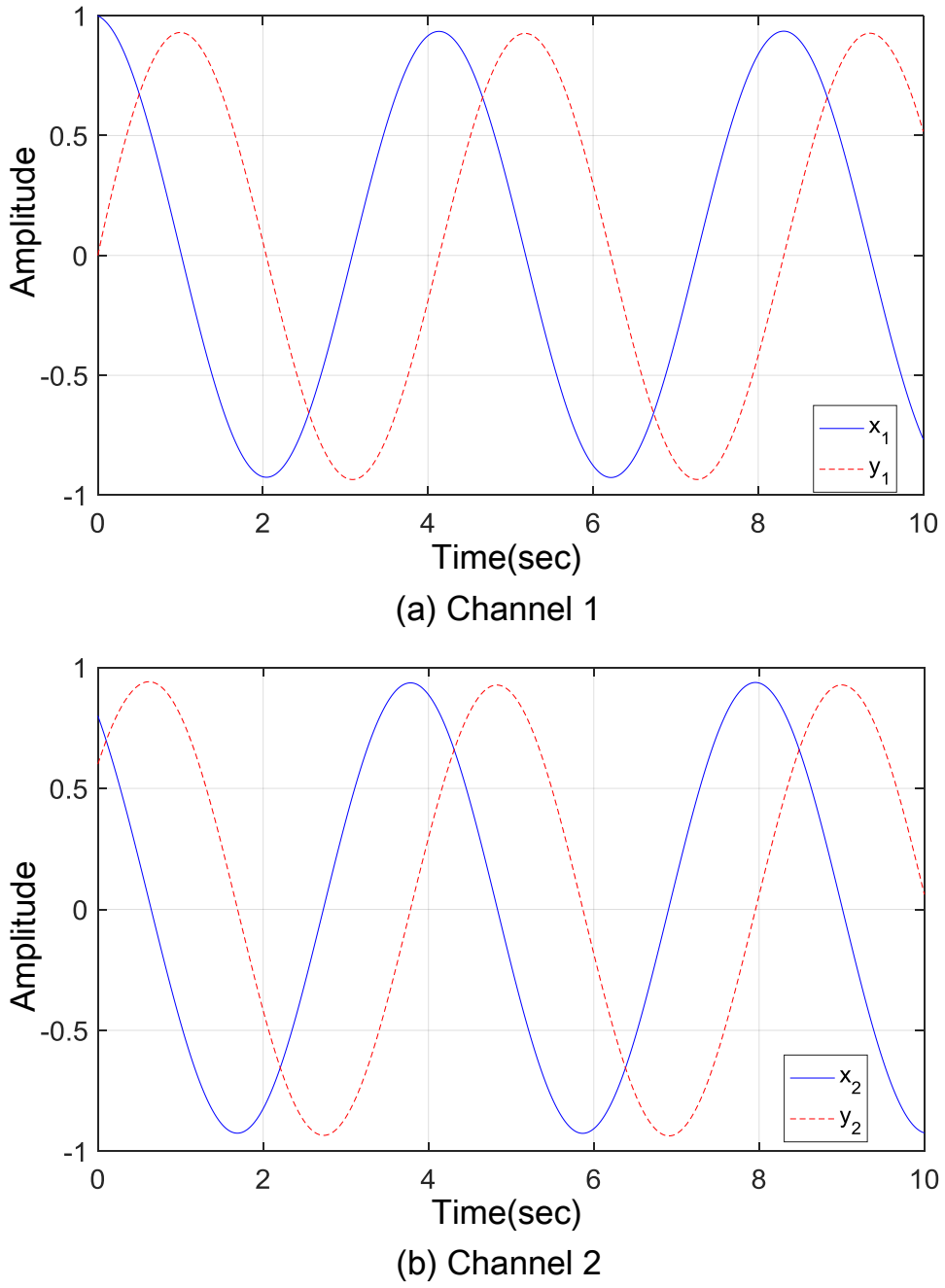

Figure 4.18: Time domain response of our oscillator.

Next, we compare the time domain response of our circuit to that from Simulink in Chapter 3. We set the same parameter value for both systems. Recall that in Simulink we can set integrators' initial values directly by modifying the corresponding parameters. But in VLSI circuit the initial conditions on the capacitors are unkown. Therefore the initial conditions for the two systems are not guaranteed to be the same. Figure 4.19 shows the waveforms of x_1. The red dashed curve is the output from Simulink, and the other one is from our circuit. As we can see, both systems are oscillating at exactly the same frequency and amplitude. The only difference is that because of uncontrollable initial conditions in the circuit, there is a phase delay between the two systems. Recall that in Simulink we used ideal components for any mathematical function we need. But when working with VLSI, we implemented every single mathematical operation with MOSFETs. All subcircuits have nonlinearity and thus affect the final output waveforms. Therefore the output from the circuit would deviate from that from Simulink in terms of oscillating amplitude and frequency. However, the output of our circuit still matches very well to the ideal output from Simulink. In conclusion, our oscillator system designed with the VLSI circuit works perfectly as a globally coupled oscillator.

4.4 Chapter Summary

In this chapter, we discussed the design and implementation of subcircuits including integrators, multipliers, current mirrors, and transconductance amplifiers. Then we used these subcircuits to implement our globally coupled oscillator system.

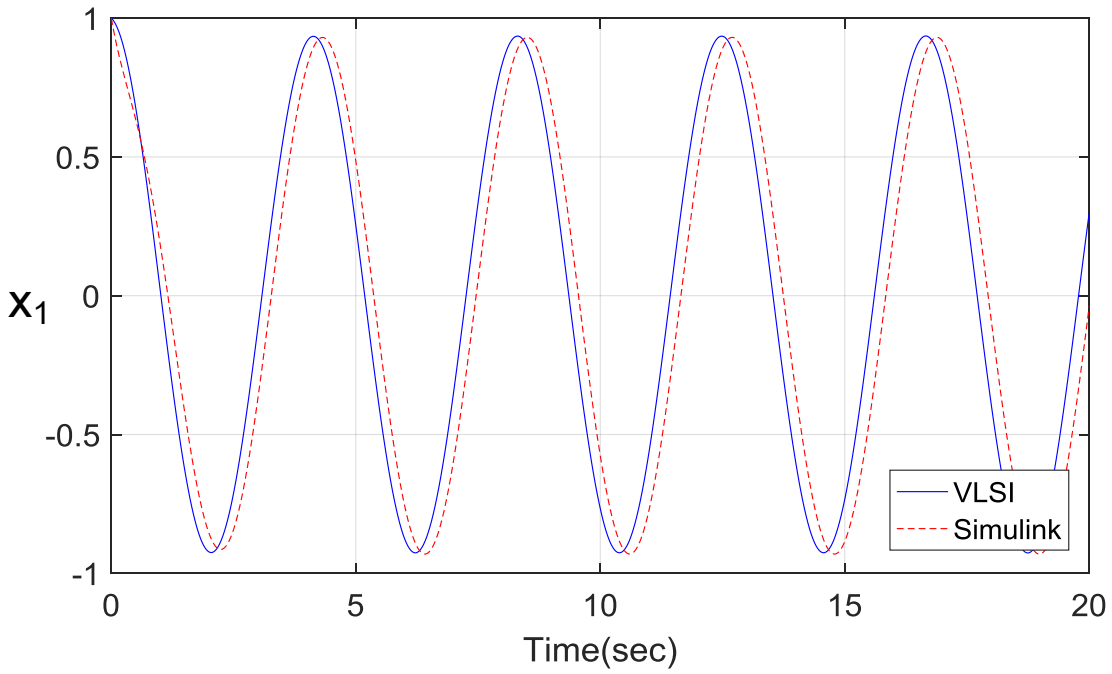

Figure 4.19: Time domain response comparison.

We also presented simulation results which showed that our system implemented with VLSI circuit works perfectly as a globally coupled oscillator.

Chapter 5: Conclusions and Future Work

5.1 Main Contributions

In this thesis we discussed the history, applications, and mathematical models of globally coupled oscillators. We also designed globally coupled oscillators using Simulink and VLSI circuits. The main contributions are listed below:

- We discussed different mathematical models of globally coupled oscillators, especially the one proposed by Matthews et al. [59]. We also analyzed the model when the number of oscillators in the system is two. Then we simulated two systems in Simulink based on our analysis.

- We proposed a VLSI design for phase synchronization of a two-channel globally coupled oscillator system. We designed all subcircuits, including integrators, multipliers, current mirrors, and transconductance amplifiers. Then we simulated the whole system in PSpice. We also presented our simulation results which showed that our system works perfectly as a globally coupled oscillator system.

5.2 Future Work

In this thesis we have designed a VLSI for a two-channel globally coupled oscillator system. There are still many things that can be done.

- Finish the layout, fabrication, and test of this system. Because of time limitation, we did not get to work on the layout of this system in order to get it fabricated. It would mean a lot if someone is to continue this project and make a real chip based on this design.

- Improve the linearity of multipliers and transconductance amplifiers. Although we have got very good simulation results, the linearity can be further improved. Currently there is still a tiny variation in the oscillating amplitude when the system becomes stable. This is due to the nonlinearity of multipliers and transconductance amplifiers. If we can further improve their linearity, the performance of the whole system will be enhanced.

- Immigrate this design to a more up to date technology. We used ON Semiconductor's 0.5 μm CMOS technology because it was available to us. But actually this technology is very old. A newer technology with smaller feature size has many advantages such as less parasitic capacitance, smaller area, and so on. Therefore, working with a more up to date technology may give our circuits better linearity and thus give the system better performance.

Appendix A: Transistor Sizes

Table A.1: All Transistors' Sizes

Figure Number	Transistor	Width (μm)	Length (μm)
Figure 4.6	M_1– M_6	1	2
	M_7	30	1
	M_8–M_{10}	2	2
	M_{11}	1	1
	M_{12}, M_{18}, M_{22}, M_{28}	2	1
	M_{13}, M_{19}, M_{23}, M_{29}	14	2
	M_{14}, M_{16}, M_{24}, M_{26}	1	10
	M_{15}, M_{17}, M_{25}, M_{27}	1	6
	M_{20}, M_{21}	40	40
Figure 4.8	M_1–M_4	1	60
	M_5–M_{12}	20	40
Figure 4.15	M_1–M_2	1	10
	M_3–M_{10}	40	40
	M_{11}–M_{14}	1	50
	M_{15}	1	1
	M_{16}–M_{17}	1	4
	M_{18}	2	1
	M_{19}	35	2

Bibliography

[1] Henrique M Oliveira and Luís V Melo. Huygens synchronization of two clocks. *Scientific Reports*, 5, 2015.

[2] Steven H Strogatz, Ian Stewart, et al. Coupled oscillators and biological synchronization. *Scientific American*, 269(6):102–109, 1993.

[3] Arkady Pikovsky and Michael Rosenblum. Dynamics of globally coupled oscillators: Progress and perspectives. *Chaos: An Interdisciplinary Journal of Nonlinear Science*, 25(9):097616, 2015.

[4] Engelbert Kaempfer, Simon Delboe, Hamond Gibben, and William Ramsden. *The history of Japan: together with a description of the kingdom of Siam, 1690-92*, volume 2. J. MacLehose and Sons, 1906.

[5] Renato E Mirollo and Steven H Strogatz. Synchronization of pulse-coupled biological oscillators. *SIAM Journal on Applied Mathematics*, 50(6):1645–1662, 1990.

[6] John Bonner Buck. Synchronous rhythmic flashing of fireflies. *The Quarterly Review of Biology*, 13(3):301–314, 1938.

[7] John Buck and Elisabeth Buck. Biology of synchronous flashing of fireflies. *Nature*, 211:562–564, 1966.

[8] John Buck and Elisabeth Buck. Mechanism of rhythmic synchronous flashing of fireflies. *Science*, 159(3821):1319–1327, 1968.

[9] John Buck. Synchronous rhythmic flashing of fireflies. ii. *The Quarterly Review of Biology*, 63(3):265–289, 1988.

[10] John Buck. Synchronous fireflies. *Scientific American*, 234:74–85, 1976.

[11] Wayne Garver and Frank Moss. Electronic fireflies. *Scientific American*, 269:128–130, 1993.

[12] Robin Meier and Andre Gwerder. Synchronizing fireflies. https://www.youtube.com/watch?v=ZGvtnE1Wy6U, 2016.

[13] Steven J Portugal, Tatjana Y Hubel, Johannes Fritz, Stefanie Heese, Daniela Trobe, Bernhard Voelkl, Stephen Hailes, Alan M Wilson, and James R Usherwood. Upwash exploitation and downwash avoidance by flap phasing in ibis formation flight. *Nature*, 505(7483):399–402, 2014.

[14] Martha K McClintock. Menstrual synchorony and suppression. *Nature*, 229(5282):244–245, 1971.

[15] James J Collins and Ian N Stewart. Coupled nonlinear oscillators and the symmetries of animal gaits. *Journal of Nonlinear Science*, 3(1):349–392, 1993.

[16] Yozo Fujino, Benito M Pacheco, Shun-Ichi Nakamura, and Pennung Warnitchai. Synchronization of human walking observed during lateral vibration of a congested pedestrian bridge. *Earthquake Engineering & Structural Dynamics*, 22(9):741–758, 1993.

[17] Steven H Strogatz, Daniel M Abrams, Allan McRobie, Bruno Eckhardt, and Edward Ott. Theoretical mechanics: Crowd synchrony on the Millennium Bridge. *Nature*, 438(7064):43–44, 2005.

[18] Pat Dallard, Tony Fitzpatrick, Anthony Flint, Angus Low, Roger Ridsdill Smith, Michael Willford, and Mark Roche. London millennium bridge: pedestrian-induced lateral vibration. *Journal of Bridge Engineering*, 6(6):412–417, 2001.

[19] Shun-ichi Nakamura and Yozo Fujino. Lateral vibration on a pedestrian cable-stayed bridge. *Structural Engineering International*, 12(4):295–300, 2002.

[20] Kenichi Hirosawa, Seiichi Kittaka, Yu Oishi, Fumihiko Kannari, and Takayuki Yanagisawa. Phase locking in a Nd: YVO 4 waveguide laser array using Talbot cavity. *Optics Express*, 21(21):24952–24961, 2013.

[21] HG Winful and SS Wang. Stability of phase locking in coupled semiconductor laser arrays. *Applied Physics Letters*, 53(20):1894–1896, 1988.

[22] Rajarshi Roy and K Scott Thornburg Jr. Experimental synchronization of chaotic lasers. *Physical Review Letters*, 72(13):2009, 1994.

[23] John R Terry, K Scott Thornburg Jr, David J DeShazer, Gregory D VanWiggeren, Shiqun Zhu, Peter Ashwin, and Rajarshi Roy. Synchronization of chaos in an array of three lasers. *Physical Review E*, 59(4):4036, 1999.

[24] Herbert G Winful and Lutfur Rahman. Synchronized chaos and spatiotemporal chaos in arrays of coupled lasers. *Physical Review Letters*, 65(13):1575, 1990.

[25] SP Benz and CJ Burroughs. Coherent emission from two-dimensional Josephson junction arrays. *Applied Physics Letters*, 58(19):2162–2164, 1991.

[26] P Hadley, MR Beasley, and K Wiesenfeld. Phase locking of Josephson-junction series arrays. *Physical Review B*, 38(13):8712, 1988.

[27] Kurt Wiesenfeld, Pere Colet, and Steven H Strogatz. Synchronization transitions in a disordered josephson series array. *Physical Review Letters*, 76(3):404, 1996.

[28] Yoshiki Kuramoto. *Chemical oscillations, waves, and turbulence*, volume 19. Springer Science & Business Media, 2012.

[29] István Z Kiss, Vilmos Gáspár, and John L Hudson. Experiments on synchronization and control of chaos on coupled electrochemical oscillators. *The Journal of Physical Chemistry B*, 104(31):7554–7560, 2000.

[30] István Z Kiss and John L Hudson. Phase synchronization of nonidentical chaotic electrochemical oscillators. *Physical Chemistry Chemical Physics*, 4(12):2638–2647, 2002.

[31] Nadia Mazouz, Katharina Krischer, Georg Flätgen, and Gerhard Ertl. Synchronization and pattern formation in electrochemical oscillators: Model calculations. *The Journal of Physical Chemistry B*, 101(14):2403–2410, 1997.

[32] Wen Wang, István Z Kiss, and JL Hudson. Experiments on arrays of globally coupled chaotic electrochemical oscillators: Synchronization and clustering. *Chaos: An Interdisciplinary Journal of Nonlinear Science*, 10(1):248–256, 2000.

[33] Ai Hasegawa, Kazuo Okanoya, Toshikazu Hasegawa, and Yoshimasa Seki. Rhythmic synchronization tapping to an audio–visual metronome in budgerigars. *Scientific Reports*, 1:120, 2011.

[34] Erik Andreas Martens, Shashi Thutupalli, Antoine Fourrière, and Oskar Hallatschek. Chimera states in mechanical oscillator networks. *Proceedings of the National Academy of Sciences*, 110(26):10563–10567, 2013.

[35] Constance Hammond, Hagai Bergman, and Peter Brown. Pathological synchronization in Parkinson's disease: networks, models and treatments. *Trends in Neurosciences*, 30(7):357–364, 2007.

[36] Xinmin Liu and Tetsuya Iwasaki. Design of coupled harmonic oscillators for synchronization and coordination. *IEEE Transactions on Automatic Control*, PP:1, 2017.

[37] Arthur T Winfree. Biological rhythms and the behavior of populations of coupled oscillators. *Journal of Theoretical Biology*, 16(1):15–42, 1967.

[38] Arthur T Winfree. The geometry of biological time. *Springer Study Edition*, 1980.

[39] Juan A Acebrón, Luis L Bonilla, Conrad J Pérez Vicente, Félix Ritort, and Renato Spigler. The Kuramoto model: A simple paradigm for synchronization phenomena. *Reviews of Modern Physics*, 77(1):137, 2005.

[40] Joel T Ariaratnam and Steven H Strogatz. Phase diagram for the Winfree model of coupled nonlinear oscillators. *Physical Review Letters*, 86(19):4278, 2001.

[41] Yoshiki Kuramoto. Self-entrainment of a population of coupled non-linear oscillators. In *International Symposium on Mathematical Problems in Theoretical Physics*, pages 420–422. Springer, 1975.

[42] MK Stephen Yeung and Steven H Strogatz. Time delay in the Kuramoto model of coupled oscillators. *Physical Review Letters*, 82(3):648, 1999.

[43] Ali Jadbabaie, Nader Motee, and Mauricio Barahona. On the stability of the Kuramoto model of coupled nonlinear oscillators. In *American Control Conference, 2004. Proceedings of the 2004*, volume 5, pages 4296–4301. IEEE, 2004.

[44] Kurt Wiesenfeld, Pere Colet, and Steven H Strogatz. Frequency locking in josephson arrays: Connection with the Kuramoto model. *Physical Review E*, 57(2):1563, 1998.

[45] Giovanni Filatrella, Arne Hejde Nielsen, and Niels Falsig Pedersen. Analysis of a power grid using a Kuramoto-like model. *The European Physical Journal B-Condensed Matter and Complex Systems*, 61(4):485–491, 2008.

[46] Erik Andreas Martens, E Barreto, SH Strogatz, E Ott, P So, and TM Antonsen. Exact results for the Kuramoto model with a bimodal frequency distribution. *Physical Review E*, 79(2):026204, 2009.

[47] Michael Breakspear, Stewart Heitmann, and Andreas Daffertshofer. Generative models of cortical oscillations: neurobiological implications of the Kuramoto model. *Frontiers in Human Neuroscience*, 4:190, 2010.

[48] Yu Maistrenko, O Popovych, O Burylko, and PA Tass. Mechanism of desynchronization in the finite-dimensional Kuramoto model. *Physical Review Letters*, 93(8):084102, 2004.

[49] Renato E Mirollo and Steven H Strogatz. The spectrum of the locked state for the Kuramoto model of coupled oscillators. *Physica D: Nonlinear Phenomena*, 205(1):249–266, 2005.

[50] Diego Pazó. Thermodynamic limit of the first-order phase transition in the Kuramoto model. *Physical Review E*, 72(4):046211, 2005.

[51] JL van Hemmen and WF Wreszinski. Lyapunov function for the Kuramoto model of nonlinearly coupled oscillators. *Journal of Statistical Physics*, 72(1):145–166, 1993.

[52] David Cumin and CP Unsworth. Generalising the Kuramoto model for the study of neuronal synchronisation in the brain. *Physica D: Nonlinear Phenomena*, 226(2):181–196, 2007.

[53] Yuri L Maistrenko, Borys Lysyansky, Christian Hauptmann, Oleksandr Burylko, and Peter A Tass. Multistability in the Kuramoto model with synaptic plasticity. *Physical Review E*, 75(6):066207, 2007.

[54] Renato Mirollo and Steven H Strogatz. The spectrum of the partially locked state for the Kuramoto model. *Journal of Nonlinear Science*, 17(4):309–347, 2007.

[55] Hyunsuk Hong and Steven H Strogatz. Conformists and contrarians in a Kuramoto model with identical natural frequencies. *Physical Review E*, 84(4):046202, 2011.

[56] Bidhan Chandra Bag, KG Petrosyan, and Chin-Kun Hu. Influence of noise on the synchronization of the stochastic Kuramoto model. *Physical Review E*, 76(5):056210, 2007.

[57] Pablo Monzón and Fernando Paganini. Global considerations on the Kuramoto model of sinusoidally coupled oscillators. In *Decision and Control, 2005 and 2005 European Control Conference. CDC-ECC'05. 44th IEEE Conference on*, pages 3923–3928. IEEE, 2005.

[58] Francisco A Rodrigues, Thomas K DM Peron, Peng Ji, and Jürgen Kurths. The Kuramoto model in complex networks. *Physics Reports*, 610:1–98, 2016.

[59] Paul C Matthews, Renato E Mirollo, and Steven H Strogatz. Dynamics of a large system of coupled nonlinear oscillators. *Physica D: Nonlinear Phenomena*, 52(2-3):293–331, 1991.

[60] Ahmadreza Rofougaran, Jacob Rael, Maryam Rofougaran, and Asad Abidi. A 900 MHz CMOS LC-oscillator with quadrature outputs. In *Solid-State Circuits Conference, 1996. Digest of Technical Papers. 42nd ISSCC., 1996 IEEE International*, pages 392–393. IEEE, 1996.

[61] Sander LJ Gierkink, Salvatore Levantino, Robert C Frye, Carlo Samori, and Vito Boccuzzi. A low-phase-noise 5-GHz CMOS quadrature VCO using superharmonic coupling. *IEEE Journal of Solid-State Circuits*, 38(7):1148–1154, 2003.

[62] John George Maneatis and Mark A Horowitz. Precise delay generation using coupled oscillators. *IEEE Journal of Solid-State Circuits*, 28(12):1273–1282, 1993.

[63] Yahya M Tousi, Omeed Momeni, and Ehsan Afshari. A novel CMOS high-power terahertz VCO based on coupled oscillators: Theory and implementation. *IEEE Journal of Solid-State Circuits*, 47(12):3032–3042, 2012.

[64] Ali Hajimiri and Thomas H Lee. Design issues in CMOS differential LC oscillators. *IEEE Journal of Solid-State Circuits*, 34(5):717–724, 1999.

[65] Jose Cabanillas, Laurent Dussopt, Jose M Lopez-Villegas, and Gabriel M Rebeiz. A 900 MHz low phase noise CMOS quadrature oscillator. In *Radio Frequency Integrated Circuits (RFIC) Symposium, 2002 IEEE*, pages 63–66. IEEE, 2002.

[66] JH McAuley and CD Marsden. Physiological and pathological tremors and rhythmic central motor control. *Brain*, 123(8):1545–1567, 2000.

[67] Rodolfo R Llinas, Anthony A Grace, and Yosef Yarom. In vitro neurons in mammalian cortical layer 4 exhibit intrinsic oscillatory activity in the 10-to 50-Hz frequency range. *Proceedings of the National Academy of Sciences*, 88(3):897–901, 1991.

[68] Behzad Razavi. *Design of Analog CMOS Integrated Circuits*. Tata McGraw-Hill Education, 2002.

[69] M Ferrera, Y Park, L Razzari, Brent E Little, Sai T Chu, R Morandotti, DJ Moss, and J Azaña. On-chip CMOS-compatible all-optical integrator. *Nature Communications*, 1:29, 2010.

[70] Robert Rieger, Andreas Demosthenous, and John Taylor. Continuously tunable, very long time constant CMOS integrator for a neural recording implant. In *Solid-State Circuits Conference, 2003. ESSCIRC'03. Proceedings of the 29th European*, pages 441–444. IEEE, 2003.

[71] Iasonas F Triantis and Andreas Demosthenous. An improved, very long time-constant CMOS integrator for use in implantable neuroprosthetic devices. In *Proceedings of the 2005 European Conference on Circuit Theory and Design, 2005.*, volume 3, pages III–15. IEEE, 2005.

[72] Takahiro Inoue, Hideo Nakane, Yuuji Fukuju, and Edgar Sánchez-Sinencio. A design of a low-voltage current-mode fully-differential analog CMOS integrator using FG-MOSFETs and its implementation. *Analog Integrated Circuits and Signal Processing*, 32(3):249–256, 2002.

[73] Robert Rieger, Andreas Demosthenous, and John Taylor. A 230-nW 10-s time constant CMOS integrator for an adaptive nerve signal amplifier. *IEEE Journal of Solid-State Circuits*, 39(11):1968–1975, 2004.

[74] Hermann Schmid. A transistorized four-quadrant time-division multiplier with an accuracy of 0.1 per cent. *IEEE Transactions on Electronic Computers*, 1(EC-7):41–47, 1958.

[75] Barrie Gilbert. A precise four-quadrant multiplier with subnanosecond response. *IEEE Journal of Solid-State Circuits*, 3(4):365–373, 1968.

[76] Joseph N Babanezhad and Gabor C Temes. A 20-V four-quadrant CMOS analog multiplier. *IEEE Journal of Solid-State Circuits*, 20(6):1158–1168, 1985.

[77] Klaas Bult and Hans Wallinga. A CMOS four-quadrant analog multiplier. *IEEE Journal of Solid-State Circuits*, 21(3):430–435, 1986.

[78] Jesus S Pena-Finol and J Alvin Connelly. A CMOS four-quadrant analog multiplier using the quarter-square technique. *IEEE Journal of Solid-State Circuits*, 22(6):1064–1073, 1987.

[79] H-J Song and C-K Kim. An CMOS four-quadrant analog multiplier using simple two-input squaring circuits with source followers. *IEEE Journal of Solid-State Circuits*, 25(3):841–848, 1990.

[80] Zhenhua Wang. A CMOS four-quadrant analog multiplier with single-ended voltage output and improved temperature performance. *IEEE Journal of Solid-State Circuits*, 26(9):1293–1301, 1991.

[81] Richard Stepp. Multiple-input four-quadrant multiplier, May 19 1992. US Patent 5,115,409.

[82] Gunhee Han and Edgar Sanchez-Sinencio. CMOS transconductance multipliers: A tutorial. *IEEE Transactions on Circuits and Systems II: Analog and Digital Signal Processing*, 45(12):1550–1563, 1998.

[83] Mark van Horn and Randall L Geiger. A CMOS OTA for voltage-controlled analog signal processing. In *Proc. IEEE Midwest Symp. on Circuits and Systems*, pages 596–599, 1985.

[84] S-C Qin and Randy L Geiger. A±5-V CMOS analog multiplier. *IEEE Journal of Solid-State Circuits*, 22(6):1143–1146, 1987.

[85] Paul R Gray and Robert G Meyer. *Analysis and Design of Analog Integrated Circuits*. John Wiley & Sons, Inc., 1990.

[86] Anand Veeravalli, Edgar Sánchez-Sinencio, and José Silva-Martínez. Transconductance amplifier structures with very small transconductances: a comparative design approach. *IEEE Journal of Solid-State Circuits*, 37(6):770–775, 2002.